Facile microwave synthesis of a Z-scheme imprinted $ZnFe_2O_4$/Ag/PEDOT with the specific recognition ability towards improving photocatalytic activity and selectivity for tetracycline

Ziyang Lu, Zehui Yu, Jinbo Dong, Minshan Song, Yang Liu, Xinlin Liu, Zhongfei Ma, Hang Su, Yongsheng Yan, Pengwei Huo

PII: S1385-8947(17)32238-6
DOI: https://doi.org/10.1016/j.cej.2017.12.115
Reference: CEJ 18276

To appear in: *Chemical Engineering Journal*

Received Date: 14 September 2017
Revised Date: 20 December 2017
Accepted Date: 22 December 2017

Please cite this article as: Z. Lu, Z. Yu, J. Dong, M. Song, Y. Liu, X. Liu, Z. Ma, H. Su, Y. Yan, P. Huo, Facile microwave synthesis of a Z-scheme imprinted $ZnFe_2O_4$/Ag/PEDOT with the specific recognition ability towards improving photocatalytic activity and selectivity for tetracycline, *Chemical Engineering Journal* (2017), doi: https://doi.org/10.1016/j.cej.2017.12.115

Facile microwave synthesis of a Z-scheme imprinted $ZnFe_2O_4$/Ag/PEDOT with the specific recognition ability towards improving photocatalytic activity and selectivity for tetracycline

Ziyang Lu,[a,b] Zehui Yu,[a] Jinbo Dong,[c] Minshan Song,[d] Yang Liu,[e] Xinlin Liu,[f] Zhongfei Ma,[a] Hang Su,[c] Yongsheng Yan[*,b] and Pengwei Huo[*,b]

a. School of the Environment and Safety Engineering, Jiangsu University, Jiangsu, Zhenjiang 212013, PR China

b. School of Chemistry & Chemical Engineering, Jiangsu University, Jiangsu, Zhenjiang 212013, PR China

c. Zhenjiang Water Corporation, Jiangsu, Zhenjiang 212003, PR China

d. School of Science, Jiangsu University of Science and Technology, Jiangsu, Zhenjiang 212003, PR China

e. Key Laboratory of Functional Materials Physics and Chemistry of the Ministry of Education, Jilin Normal University, Jilin, Changchun 130103, PR China

f. School of Energy and Power Engineering, Jiangsu University, Jiangsu, Zhenjiang 212013, PR China

Abstract

The Z-scheme imprinted $ZnFe_2O_4$/Ag/PEDOT was synthesized by the microwave polymerization method and surface imprinting technique, which possessed good partial hollow spherical structure, good light response ability, good magnetic separation performance, good photocatalytic stability and reproducibility. More importantly, due to the introduction of Ag/PEDOT into the surface imprinted layer, Z-scheme structure was formed to enhance the photocatalytic activity based on Ag acted as the mediator, meanwhile, owing to the existence of the imprinted cavity in the surface imprinted layer, the selectivity had been significantly improved, in a word, the as-prepared Z-scheme imprinted $ZnFe_2O_4$/Ag/PEDOT achieved the goal for simultaneously improving the photocatalytic activity and selectivity. Z-scheme imprinted

[*] Corresponding author. E-mail: luziyang126@126.com (Y.S. Yan), huopw@mail.ujs.edu.cn (P.W. Huo). Tel.: +86–0511–88791800; Fax: +86–0511–88791800.

$ZnFe_2O_4$/Ag/PEDOT possessed the highest photodegradation rate (71.77 %) for degradation of tetracycline under the simulated sunlight irradiation of 120 min, which was approximately 4.74 times to that of $ZnFe_2O_4$, 1.42 times to that of Ag/PEDOT and 1.31 times to that of non-imprinted $ZnFe_2O_4$/Ag/PEDOT, respectively. And the coefficient of selectivity of Z-scheme imprinted $ZnFe_2O_4$/Ag/PEDOT relative to $ZnFe_2O_4$, Ag/PEDOT, non-imprinted $ZnFe_2O_4$/Ag/PEDOT was 1.84, 1.82, 1.79 in the single antibiotic solution and 1.78, 1.75, 1.67 in the binary antibiotic solution, respectively. This work provided a new synthesis strategy for the imprinted photocatalysts and also provided a new idea for the treatment of specific pollutants in the water environment.

Keywords: Microwave polymerization method; Z-scheme structure; Surface imprinting technique; Specific recognition ability; Improved photocatalytic activity and selectivity

1. Introduction

Recently, the problem of water pollution is becoming more and more serious along with the rapid development of industry [1-5]. Tetracycline (TC), as one of the most widely used antibiotics, produces more and more residues in the water environment, which is a serious threat to the ecological environment and human health [6-9]. Therefore, finding a quick and effective method to remove TC residues from the water environment has caused widespread concern [10]. Currently, photocatalysis as a green technology which uses light energy and degrades pollutants to non–toxic harmless substances, has aroused great interest among many scholars [11-15].

Nowadays, CdS, TiO_2 and ZnO have been extensively studied as the common semiconductor photocatalysts [16-22], which have their respective advantages. However, the poor reproducibility also severely restricts the development and application of above common semiconductor photocatalysts [23, 24], consequently, $ZnFe_2O_4$, as a potential candidate for photocatalysis, has been widely used owing to its narrow band gap (1.9 eV), low toxicity, good stability and excellent ferromagnetic properties for magnetic separation from the aqueous solution [25-29].

Nevertheless, the common defect of all above photocatalysts (such as poor selectivity) is also evident, as we know, the produced h^+, $\cdot OH$ and $\cdot O_2^-$ act non-selectively to destroy all organic pollutants, and these photocatalysts can not selectively remove the specific pollutant (such as very high toxic pollutant) in the presence of other pollutants (such as some low toxic or non-toxic

pollutants) [30-33], this defect greatly limits their functional application. In order to overcome above defect, surface imprinting technique, as an effective approach for synthesizing materials with the specific recognition ability towards the target molecule by using the imprinted cavity, is introduced to improve the selectivity [34-38], because the surface imprinted materials possess the excellent specific recognition ability to selectively adsorb the specific high toxic target molecule to the imprinted cavity in the presence of other low toxic or non-toxic pollutants, and then the specific high toxic target molecule adsorbed in the imprinted cavity can be further degraded to the intermediates, afterwards, due to the fact that these degradation intermediates are still in the imprinted cavity and it is not fast to go out of the imprinted cavity, these degradation intermediates can be continued to be degraded. However, if the common photocatalysts are coated with a surface imprinted layer, the selectivity will improve, but the photocatalytic activity will greatly reduce owing to the cover of the surface imprinted layer [39], accordingly, how to improve selectivity without reducing photocatalytic activity is a great challenge.

Based on above considerations, we find that conductive polymer (a typical organic semiconductor) can be introduced into the surface imprinted layer as a functional monomer, such as poly-3,4-ethylenedioxythiophene (PEDOT). PEDOT [40, 41], as a typical conductive polymer, not only has good photocatalytic activity, but also can be used as the functional monomer for synthesizing the surface imprinted layer. More importantly, compared with the traditional imprinted photocatalytic method (coating the imprinted layer on the semiconductors), the introduction of PEDOT into the surface imprinted layer not only can significantly improve the selectivity, but also can effectively avoid the decrease of photocatalytic activity resulting from the cover of the surface imprinted layer on the semiconductor photocatalysts. In addition, in order to further enhance the photocatalytic activity, noble metal (silver, Ag) [42-46] is used to load on PEDOT. Ag can be used as the mediator to form the Z-scheme photocatalyst [47-50], which can effectively transfer the photo-generated electrons generating from PEDOT and photo-induced holes generating from $ZnFe_2O_4$ under the light irradiation. In short, the introduction of Ag/PEDOT as the functional monomer into the surface imprinted layer not only improves the selectivity, but also enhances the photocatalytic activity. Up to now, no work has been reported in this respect.

What's more, the conventional polymerization methods (such as: thermal polymerization [51, 52] and UV light polymerization [14, 53]) have their respective shortcomings of poor activity and

long reaction time for thermal polymerization, poor activity and poor stability for UV light polymerization. According to the literature survey and experimental result, microwave polymerization [39, 54] is a facile and efficient method to synthesize the imprinted polymer and supply these shortcomings of poor activity, long reaction time and poor stability, especially, microwave polymerization is a good method for synthesizing materials with spherical structure. To our knowledge, no literature has been reported about this Z-scheme imprinted $ZnFe_2O_4$/Ag/PEDOT.

Therefore, in this work, based on $ZnFe_2O_4$ as the carrier and Ag/PEDOT as the functional monomer, the Z-scheme imprinted $ZnFe_2O_4$/Ag/PEDOT was synthesized via the microwave polymerization method and surface imprinting technique. A series of characterizations and influence factors were investigated to confirm the composition, structure, morphology and performance. The corresponding adsorption, photocatalysis, selectivity and reproducibility were also investigated. What's more, the photodegradation intermediates, specific recognition and selective photocatalytic mode were thoroughly illustrated through getting insight into the mechanism.

2. Experimental section

2.1 Materials

Zinc chloride ($ZnCl_2$, A.R.), ferric chloride hydrate ($FeCl_3 \cdot 6H_2O$, A.R.), iron(III) chloride ($FeCl_3$, A.R.), ammonium acetate (A.R.), trimethylolpropane trimethacrylate (TRIM, A.R.), 2,2'-azobis(2-methylpropionitrile) (AIBN, 98 %), Aerosol OT (AOT, 96 %), 3,4-ethylenedioxythiophene (EDOT, 99 %), tert-butyl alcohol (t-BuOH, A.R.), triethanolamine (TEOA, A.R.), benzoquinone (BQ, A.R.) and 5,5-diamethyl-1-pyrroline n-oxide (DMPO, 97 %) were all supported by Aladdin Chemistry Co., Ltd. Nitrogen (N_2) was supplied by INHONG GAS. Tetracycline (TC, 99 %) and enrofloxacin hydrochloride (EH, 99 %) were purchased from National Institutes for Food and Drug Control. Anhydrous ethanol (A.R.), n-hexane (A.R.), ethylene glycol (A.R.), silver nitrate ($AgNO_3$, A.R.), sodium borohydride ($NaBH_4$, A.R.) and dimethyl sulfoxide (DMSO, A.R.) were all supported by Sinopharm Chemical Reagent Co., Ltd. Deionized water was used throughout this work.

2.2 Synthesis

2.21 Synthesis of $ZnFe_2O_4$

Briefly, 2 mmol of $ZnCl_2$ and 4 mmol of $FeCl_3 \cdot 6H_2O$ were dissolved in 70 mL of ethylene glycol, subsequently, 30 mL of ammonium acetate was added into above clarification solution with vigorous mechanical agitation for 30 min at the room temperature. After reacting 72 h in a Teflon-lined stainless steel autoclave at 210 ^oC, the autoclave was cooled to the room temperature. Afterwards, the solid product was washed with anhydrous ethanol and deionized water for several times. Finally, after drying under vacuum at 40 ^oC, $ZnFe_2O_4$ was obtained.

2.22 Synthesis of Ag/PEDOT

PEDOT was synthesized as follows: 3.8 g of AOT was dissolved in 15 mL of n-hexane, afterwards, 0.47 mL 10.2 mol L^{-1} of $FeCl_3$ solution was added into above mixed solution with mechanical agitation to form the reverse micellar solution. Subsequently, 0.45 g of EDOT was added into above solution, after ultrasonic for 10 min and further mechanical agitation for 12 h at the room temperature, the solid product was washed with anhydrous ethanol for several times. Finally, after drying under vacuum at 40 ^oC, poly-3,4-ethylenedioxythiophene (PEDOT) was obtained.

In the following step, Ag/PEDOT was synthesized as follows: 1.45 g of PEDOT was added into 320 mL 0.025 mol L^{-1} of $AgNO_3$ solution with mechanical agitation for 60 min at the room temperature. Subsequently, 380 mL 0.025 mol L^{-1} of $NaBH_4$ solution was added into above mixed solution drop by drop, after reacting 90 min under the mechanical agitation, the product was washed with deionized water for several times and then dried under vacuum at 40 ^oC. In consequence, Ag/PEDOT was obtained.

2.23 Synthesis of Z-scheme imprinted $ZnFe_2O_4$/Ag/PEDOT

Z-scheme imprinted $ZnFe_2O_4$/Ag/PEDOT was synthesized via the microwave polymerization method and surface imprinting technique, the specific process was as follows: 0.01 g of Ag/PEDOT and 0.1 g of $ZnFe_2O_4$ were added into 20 mL of DMSO with the magnetic stirring for 30 min at 90 ^oC, after adding 0.05 mmol of TC, the mixed solution was stored under a N_2 atmosphere for 12 h without light. Afterwards, 0.5 mL of TRIM and 0.01 g of AIBN were both added into above mixed solution, the polymerization reaction was carried out in the microwave synthesizer (XH-300UL, Beijing XiangHu Science and Technology Development Lo., Ltd) at 700W and 60 ^oC. After reacting 1 h, the product was washed with anhydrous ethanol and

deionized water for several times. Subsequently, the molecular template (TC) was removed by adding 200 mL deionized water into above solution under the simulated sunlight irradiation (250 W xenon lamp) for 2 h with the magnetic agitation at the room temperature under an air atmosphere. Finally, the solid product was washed with anhydrous ethanol and deionized water for several times, after drying under vacuum at 40 ^{o}C, Z-scheme imprinted $ZnFe_2O_4$/Ag/PEDOT was obtained. The whole scheme of the synthesis approach was showed in Scheme. 1.

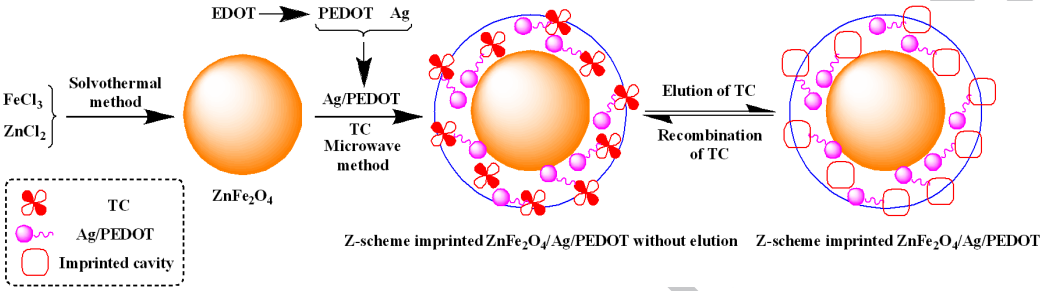

Scheme. 1 the whole scheme of the synthesis approach

2.24 Synthesis of non-imprinted $ZnFe_2O_4$/Ag/PEDOT

The synthesis process of non-imprinted $ZnFe_2O_4$/Ag/PEDOT was consistent with that of Z-scheme imprinted $ZnFe_2O_4$/Ag/PEDOT, but without the adding and the removal process of TC.

2.3 Characterization

XRD patterns were obtained with a D8 ADVANCE X-ray diffractometer (Bruker AXS Co., Germany). Fourier-transformed infrared (FT-IR) spectra of the samples were recorded on a Nicolet Nexus 470 FT-IR (Thermo Nicolet Co., USA) with 2.0 cm^{-1} resolution in the range 400 cm^{-1} - 4000 cm^{-1}, using KBr pellets. The morphology was observed by a JEM-2010 transmission electron microscope (TEM, Japan) and a JSM-7001F scanning electron microscopy (SEM, Japan) equipped with the energy dispersive spectroscopy analysis (EDS). X-ray photoelectron spectroscopy (XPS) was measured with a PHI5300 spectrometer using Al K (12.5 kV) X-ray source. Magnetic measurement was carried out using a vibrating sample magnetometer (VSM) (7300, Lakeshore) under a magnetic field up to 10 kOe. The specific surface area, pore volume and average pore diameter of the samples were measured by using a NOVA 4000e high speed automated surface area and pore size analyzer (Quantachrome Co., USA). UV-vis diffused reflectance spectra (UV-vis DRS) were obtained for the dry-pressed disk samples using 2450 spectrometer (Shimazu Co., Japan) equipped with the integrated sphere accessory for diffused

reflectance spectra, using $BaSO_4$ as the reflectance sample. The degradation course of DM was monitored by Thermo LXQ mass spectrometry (MS). The total organic carbon content (TOC) was measured and analyzed by multi N/C 2100 TOC total organic carbon analyzer (Germany). Electron spin resonance (ESR) spectroscopy was carried on a Bruker A300 ESR spectrometer at room temperature.

2.4 Adsorption experiment

The adsorption performance was carried out in the dark at 30 ^{o}C with the magnetic stirring (600 rpm/min). 0.02 g of sample was added into 100 mL 20 mg L^{-1} of TC solution, afterwards, the sample analysis was carried out at interval of 10 min until 60 min, and the concentration was measured with a UV-vis spectrophotometer 2450 (Shimadzu Co., Japan). The adsorption capacity (Q) was calculated by using the formula:

$$Q = \frac{(C_0 - C) \times V}{m} \quad (1)$$

Where C_0 is the initial concentration of TC, C is the concentration of TC after adsorbing, V is the volume of the TC solution, and m is the mass of the sample.

2.5 Photocatalytic experiment

The photocatalytic performance was carried out under an air atmosphere (the aeration rate was 2 mL min^{-1}) with the magnetic stirring (600 rpm/min) at 30 ^{o}C and the simulated sunlight irradiation provided by a 250 W xenon lamp (the illuminance was 1.8×10^5 lux). Briefly, 0.02 g of sample was added into 100 mL 20 mg L^{-1} of TC solution. After reaching the desired adsorption time in the dark, the mixed solution was irradiated at interval of 20 min until 120 min, and the concentration was measured with the UV-vis spectrophotometer 2450. The photodegradation rate was calculated by using the formula:

$$\text{Photodegradation rate} = \left(1 - \frac{C}{C_0}\right) \times 100\% \quad (2)$$

Where C_0 is the initial concentration of TC after adsorbing and C is the concentration of TC after irradiating.

2.6 Selective experiment

The selectivity for degradation of the single antibiotic solution was carried out in accordance with part 2.5, but before the start of the reaction, 100 mL 20 mg L^{-1} of TC solution was replaced by 100 mL 20 mg L^{-1} of EH solution. The selectivity coefficient ($k_{selectivity}$) was calculated by using

the formula:

For imprinted sample:

$$k_{imprinted} = \frac{\text{photodegradation rate (TC)}}{\text{photodegradation rate (EH)}} \quad (3)$$

For other samples:

$$k_{others} = \frac{\text{photodegradation rate (TC)}}{\text{photodegradation rate (EH)}} \quad (4)$$

For the selectivity coefficient:

$$k_{selectivity} = \frac{k_{imprinted}}{k_{others}} \quad (5)$$

The selectivity for degradation of the binary antibiotic solution containing TC and EH was carried out also in accordance with part 2.5, but before the start of the reaction, 100 mL 20 mg L^{-1} of TC solution was replaced by 100 mL binary antibiotic solution which contained 20 mg L^{-1} of TC and 20 mg L^{-1} of EH. The data were measured by HPLC (Shimadzu Co., Japan) (temperature was 298 K, mobile phase was methanol–acetic acid (40/60, v/v) with a flow rate of 1 mL min^{-1}, and the wavelength λ_{max} = 276 nm). And the selectivity coefficient ($k_{selectivity}$) was also calculated according to the equation (3), (4) and (5).

2.7 Mechanism experiment

The mechanism experiment of the Z-scheme imprinted $ZnFe_2O_4$/Ag/PEDOT was also carried out in accordance with part 2.5, but before the start of the reaction, some quenchers (1 mmol) were added into the TC solution, such as TEOA, t-BuOH and BQ.

2.8 Cyclic experiment

The reproducibility of the Z-scheme imprinted $ZnFe_2O_4$/Ag/PEDOT was investigated as follows: After the first photocatalytic reaction (part 2.5), the sample was isolated by a magnet and sonicated with anhydrous ethanol for 1 h to remove the residual TC and by-products. Subsequently, the solid sample was washed with anhydrous ethanol and deionized water for several times, after drying under vacuum at 40 ^{o}C, the solid sample was performed the next photocatalytic reaction. Above procedure was repeated five times to confirm the reproducibility of the Z-scheme imprinted $ZnFe_2O_4$/Ag/PEDOT.

2.9 Electrochemical measurements

The Mott–Schottky experiments were conducted to evaluate the band positions of the Z-scheme imprinted $ZnFe_2O_4$/Ag/PEDOT. An electrochemical workstation (CHI600E/700E,

Shanghai CH Instrument Co., Ltd.) connected to a computer was used in this electrochemical experiment. The potential range was −1 V to 0.5 V with potential steps of 0.05 V at a constant frequency of 962 Hz. The as-prepared photoanode, Ag/AgCl electrode and Pt plate were employed as the working, reference and counter electrode, respectively. 0.5 M Na_2SO_4 aqueous solution (pH = 7.02) was adopted as the electrolyte.

2.10 Mineralization experiment

The mineralization experiment was carried out in accordance with part 2.5, but after the photocatalytic reaction, the solution was measured with the total organic carbon analyzer, and the mineralization rate was calculated by using the formula:

$$\text{Mineralization rate} = \left(1 - \frac{\text{organic carbon content after reaction}}{\text{total organic carbon content}}\right) \times 100\% \quad (6)$$

3. Results and discussion

3.1 Characterization

Fig. 1 presented the XRD patterns of different samples. In Fig. 1a, the diffraction peaks appeared at 2θ values of 38.2 °, 44.4 °, 64.5 ° and 77.4 ° could be indexed to the face-centered cubic Ag, which was corresponding well with the JCPDS standard card 65-2871 data file [55, 56], and the diffraction peaks at 38.2 °, 44.4 °, 64.5 ° and 77.4 ° could be marked by the indexes ((111), (200), (220) and (311)), this result demonstrated that Ag had been successfully loaded on PEDOT. Meanwhile, in Fig. 1b, all the diffraction peaks (2θ = 30.1 °, 35.4 °, 37.1 °, 43.1 °, 53.4 °, 56.9 ° and 62.5 °) were matched well the typical cubic spinel $ZnFe_2O_4$ (JCPDS standard card 22-1012), and these diffraction peaks correspond to the indexes ((220), (311), (222), (400), (422), (511) and (440)), respectively [57, 58]. Moreover, compared with $ZnFe_2O_4$, an additional diffraction peak at 38.2 ° was observed in the XRD patterns of Z-scheme imprinted $ZnFe_2O_4$/Ag/PEDOT (Fig. 1c), which was belong to the strongest diffraction peak of Ag, above results demonstrated that the crystalline structure of Ag and $ZnFe_2O_4$ was not changed during coating the surface layer.

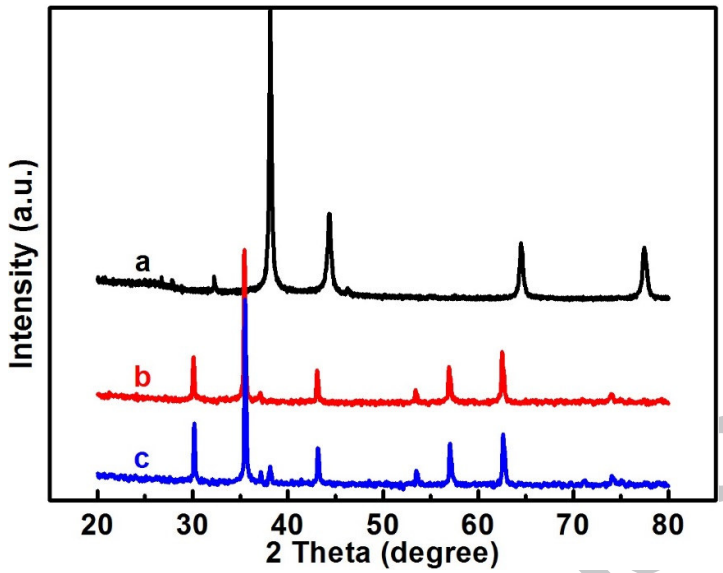

Fig. 1 XRD patterns of Ag/PEDOT (a), $ZnFe_2O_4$ (b) and Z-scheme imprinted $ZnFe_2O_4$/Ag/PEDOT (c)

In order to further prove the formation of the Z-scheme imprinted $ZnFe_2O_4$/Ag/PEDOT, FT-IR spectra of different samples were employed, which was shown in Fig. 2. Compared with $ZnFe_2O_4$, six additional absorption peaks (1716 cm^{-1}, 1641 cm^{-1}, 1331 cm^{-1}, 1197 cm^{-1}, 1076 cm^{-1} and 1973 cm^{-1}) were observed in Z-scheme imprinted $ZnFe_2O_4$/Ag/PEDOT, because of the existence of PEDOT and the surface imprinted layer. Briefly, the absorption peak of -C=O was observed at 1716 cm^{-1} [53], the absorption peak at 1641 cm^{-1} was attributed to C=C in TRIM [53] or C=C in the thiophene ring of PEDOT [59], the absorption peak of C-C and C=C in the thiophene ring of PEDOT was observed at 1331 cm^{-1} [60], the absorption peaks of C-O-C were observed at 1197 cm^{-1} and 1076 cm^{-1} [59, 60], and the absorption peak of C-S was observed at 973 cm^{-1} [60]. All above absorption peaks demonstrated that PEDOT and the surface imprinted layer were successfully formed in the as-prepared imprinted Ag/PEDOT/$ZnFe_2O_4$, and the Z-scheme imprinted $ZnFe_2O_4$/Ag/PEDOT had been successfully synthesized.

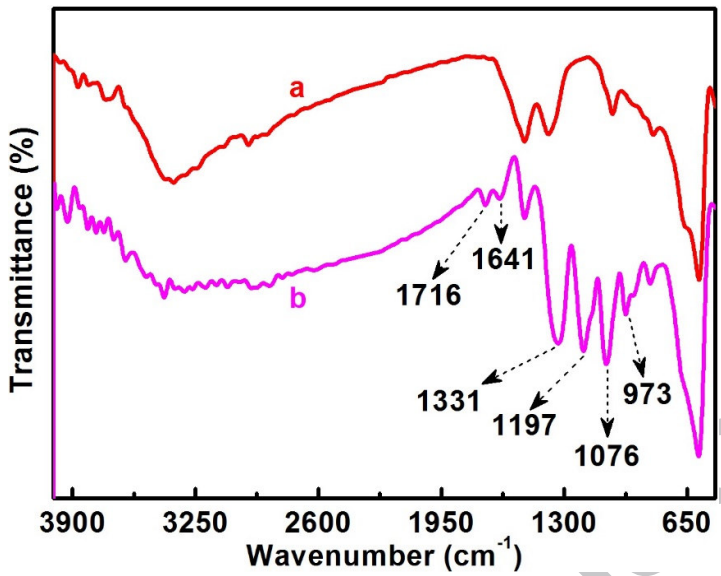

Fig. 2 FT-IR spectra of $ZnFe_2O_4$ (a) and Z-scheme imprinted $ZnFe_2O_4$/Ag/PEDOT (b)

XPS spectrum of the Z-scheme imprinted $ZnFe_2O_4$/Ag/PEDOT was further investigated to confirm the elemental composition. It could be clearly seen in Fig. 3 that Ag $3d_{5/2}$ and Ag $3d_{3/2}$ were both existed in the sample, which pointed out that the as-prepared sample possessed Ag. At the same time, Fe $2p_{3/2}$, Fe $2p_{1/2}$, Zn $2p_{3/2}$, Zn $2p_{1/2}$ and O 1s were also observed in the sample, which demonstrated that $ZnFe_2O_4$ was successfully synthesized. In addition, C 1s and N 1s indirectly indicated that PEDOT was also successfully synthesized. Therefore, above results also proved that Z-scheme imprinted $ZnFe_2O_4$/Ag/PEDOT had been successfully synthesized.

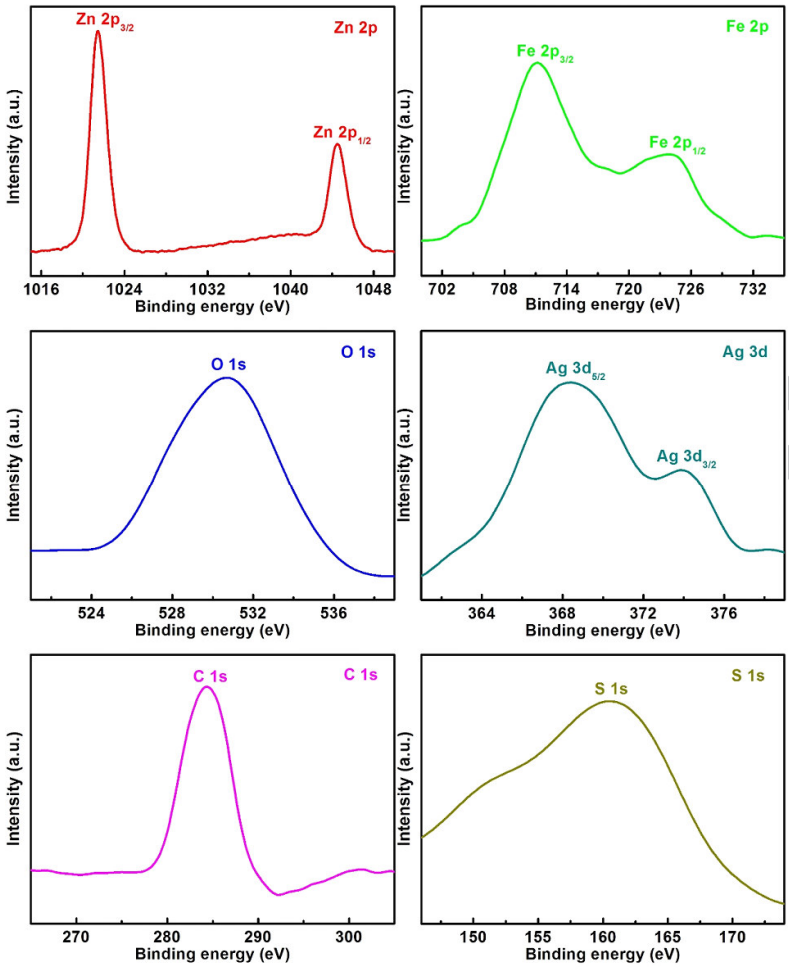

Fig. 3 XPS spectrum of the Z-scheme imprinted $ZnFe_2O_4$/Ag/PEDOT

TEM images and SEM images were employed to investigate the morphology of different samples, which were displayed in Fig. 4. It can be easily found in Fig. 4a and Fig. 4c that $ZnFe_2O_4$ possessed good partial hollow spherical structure with the average diameter of approximately 470 nm. Compared with $ZnFe_2O_4$, after coating the surface imprinted layer, an additional inhomogeneous covering layer was clearly observed on the surface of $ZnFe_2O_4$ in Fig. 4b, which indicated that the surface imprinted layer had been successfully coated on the surface of $ZnFe_2O_4$, besides, Z-scheme imprinted $ZnFe_2O_4$/Ag/PEDOT still possessed good partial hollow spherical structure and the average diameter was approximately 480 nm. Moreover, the elements of Zn, Fe and O in Fig. 4e proved again that $ZnFe_2O_4$ had been successfully synthesized, and compared with Fig. 4e, the additional elements (C, S and Ag) were observed in Fig. 4f, which indirectly proved again that Ag/PEDOT and the surface imprinted layer were both existed in the Z-scheme imprinted $ZnFe_2O_4$/Ag/PEDOT.

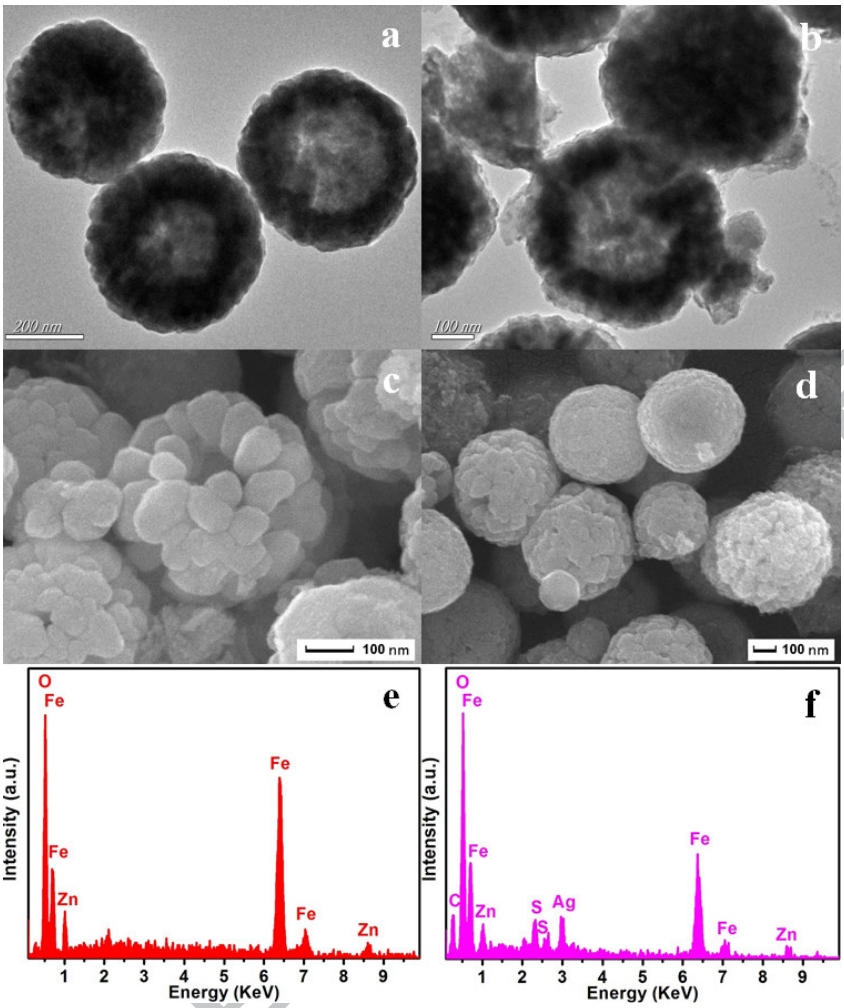

Fig. 4 TEM images, SEM images and EDS spectra of $ZnFe_2O_4$ (a, c and e) and Z-scheme imprinted $ZnFe_2O_4$/Ag/PEDOT (b, d and f)

In order to further prove that the imprinted cavities were indeed existed in the surface imprinted layer, the N_2 adsorption−desorption experiments were conducted and displayed in Fig. 5. According to relevant literatures [61, 62], the Z-scheme imprinted $ZnFe_2O_4$/Ag/PEDOT belonged to the typical IV type N_2 adsorption-desorption isotherm and H_1 type hysteresis loop, indicating that the Z-scheme imprinted $ZnFe_2O_4$/Ag/PEDOT possessed the mesoporous structure. The BET specific surface area of Z-scheme imprinted $ZnFe_2O_4$/Ag/PEDOT was 181.53 m^2 g^{-1} and its average pore diameter was 3.04 nm. Therefore, the N_2 adsorption−desorption experiments fully proved that the imprinted cavities had been formed and existed in the surface imprinted layer of Z-scheme imprinted $ZnFe_2O_4$/Ag/PEDOT.

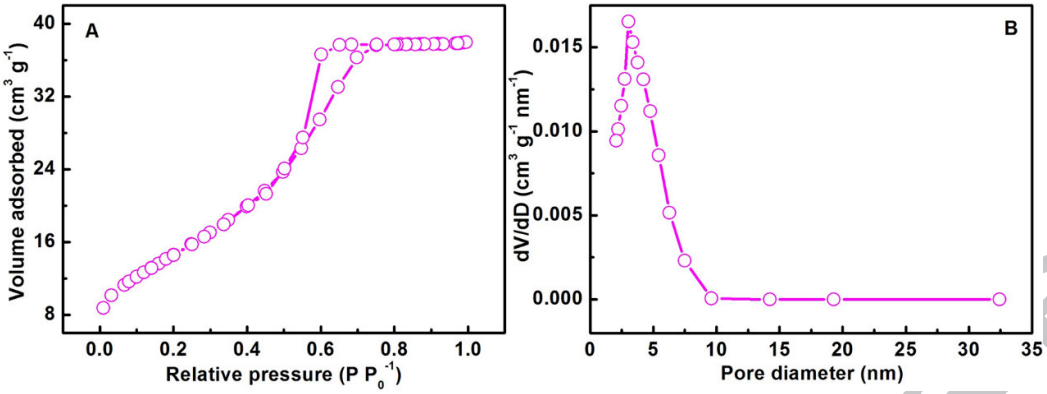

Fig. 5 N_2 adsorption-desorption isotherm (A) and corresponding pore size distribution curve (B) of the Z-scheme imprinted $ZnFe_2O_4$/Ag/PEDOT

Fig. 6A displayed the UV-vis DRS spectra of different samples. As shown in Fig. 6A, PEDOT and $ZnFe_2O_4$ both had good light response ability, and after coating the surface imprinted layer, the Z-scheme imprinted $ZnFe_2O_4$/Ag/PEDOT still exhibited good absorption in different light range. Besides, the band edge of PEDOT and $ZnFe_2O_4$ could be estimated according to the following equation, and the data were shown in Fig. 6B, Fig. 6C and Fig. 6D.

$$(Ahν)^{\frac{2}{n}}=k(hν-E_g) \quad (7)$$

Where A, h, ν, k and E_g were absorption coefficient, planck constant, light frequency, proportionality constant and band gap, respectively [63, 64].

The value of n and E_g was determined according to the literatures [65]. Briefly, plot $(Ahν)^{2/n}$ vs hν and evaluated the band gap (E_g) by extrapolating the straight line to the hν axis intercept, as shown in Fig. 6B, when n = 1, E_g of PEDOT and $ZnFe_2O_4$ was 2.21 eV and 2.03 eV, respectively. Similarly, as shown in Fig. 6C, when n = 4, E_g of PEDOT and $ZnFe_2O_4$ was 0.45 eV and 0.55 eV, respectively. Secondly, plot ln(Ahν) vs ln(hν-E_g), using the approximate E_g value of 1.61 eV for PEDOT and 1.77 eV for $ZnFe_2O_4$ in accordance of absorption spectra (Fig. 6A), afterwards, determined the value of n with the slope of the straightest line near the band edge. As shown in Fig. 6D, the slope was 1.03 for PEDOT and 0.99 for $ZnFe_2O_4$, accordingly, the corresponding value of n may be determined to 1 both for PEDOT and $ZnFe_2O_4$. Therefore, the band gap (E_g) of PEDOT and $ZnFe_2O_4$ was 2.21 eV, and 2.03 eV, respectively, and PEDOT and $ZnFe_2O_4$ were both belong to the direct transition absorption.

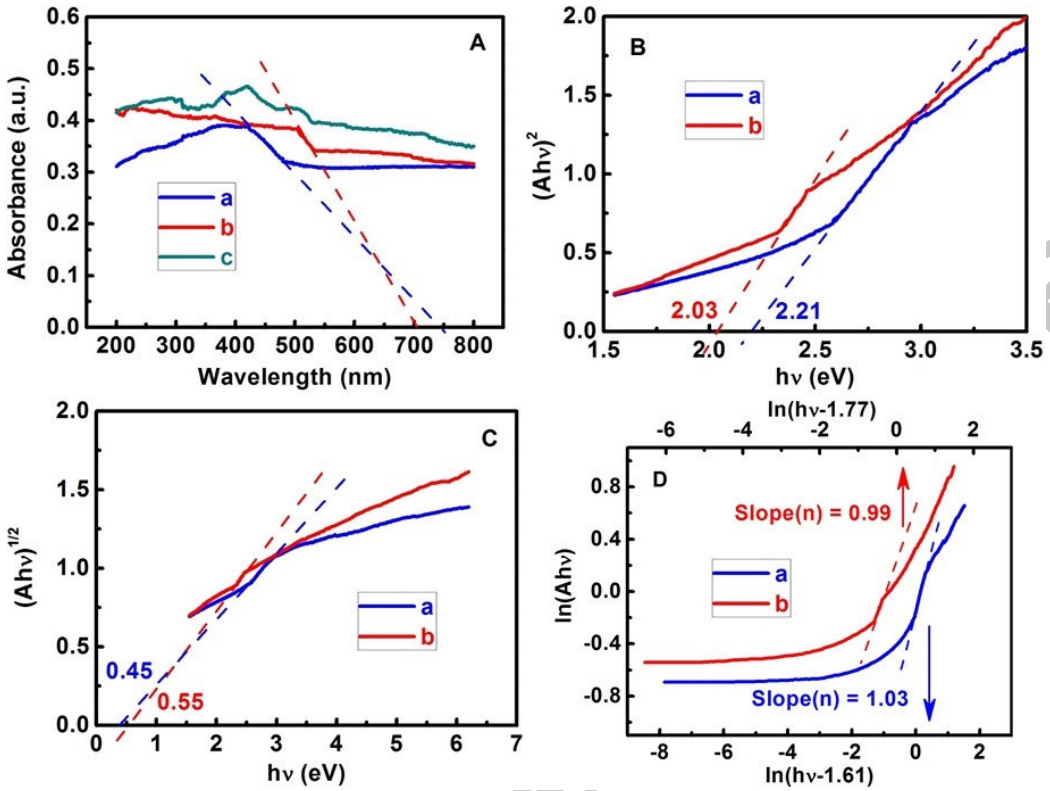

Fig. 6 UV-vis DRS spectra (A), plots of $(Ahν)^2$ versus hν (B), plots of $(Ahν)^{1/2}$ versus hν (C), plots of ln(Ahν) vs ln(hν - 1.61) for PEDOT and plots of ln(Ahν) vs ln(hν - 1.77) for $ZnFe_2O_4$ (D) of different samples (a. PEDOT, b. $ZnFe_2O_4$ and c. Z-scheme imprinted $ZnFe_2O_4$/Ag/PEDOT)

The magnetization patterns at room temperature of different samples were displayed in Fig. 7. It can be clearly seen that, compared with $ZnFe_2O_4$ (82.65 emu g^{-1}), Z-scheme imprinted $ZnFe_2O_4$/Ag/PEDOT also exhibited distinct magnetism and the magnetic saturation (Ms) value was 69.36 emu g^{-1}, indicating that the magnetism was not weakened markedly by the covering of the surface imprinted layer. The photograph (inset in Fig. 7) also proved that the Z-scheme imprinted $ZnFe_2O_4$/Ag/PEDOT could be easily separated by a magnet, indicating that the Z-scheme imprinted $ZnFe_2O_4$/Ag/PEDOT indeed possessed good magnetic separation performance.

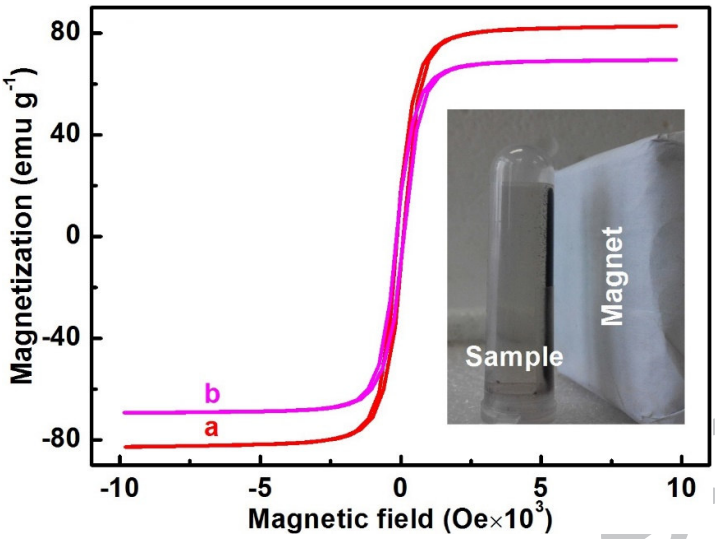

Fig. 7 Magnetization patterns at room temperature of $ZnFe_2O_4$ (a) and Z-scheme imprinted $ZnFe_2O_4$/Ag/PEDOT (b) (inset in B is the photograph of the Z-scheme imprinted $ZnFe_2O_4$/Ag/PEDOT separated from solution under a magnet)

3.2 Adsorption performance

The adsorption experiment was carried out in accordance with part 2.4. It can be easily found in Fig. 8 that the adsorption capacity of all the samples increased significantly before 30 min, and due to the fact that a lot of imprinted cavities were existed in the surface imprinted layer of Z-scheme imprinted $ZnFe_2O_4$/Ag/PEDOT, and these imprinted cavities had a strong specific recognition ability for TC, Z-scheme imprinted $ZnFe_2O_4$/Ag/PEDOT had a faster adsorption rate. While when the adsorption time was more than 30 min, the reaction process of all the samples followed the order of adsorption–desorption–adsorption, which reached the desired adsorption state for photocatalysis. Besides, compared with $ZnFe_2O_4$ and Ag/PEDOT, the Z-scheme imprinted $ZnFe_2O_4$/Ag/PEDOT possessed the highest adsorption performance, and the adsorption capacity fluctuated around 1.47 mg g^{-1} which was approximately 2.04 times to that of $ZnFe_2O_4$ and 1.48 times to that of Ag/PEDOT. Therefore, in the following experiments, 30 min was chosen as the desired adsorption time.

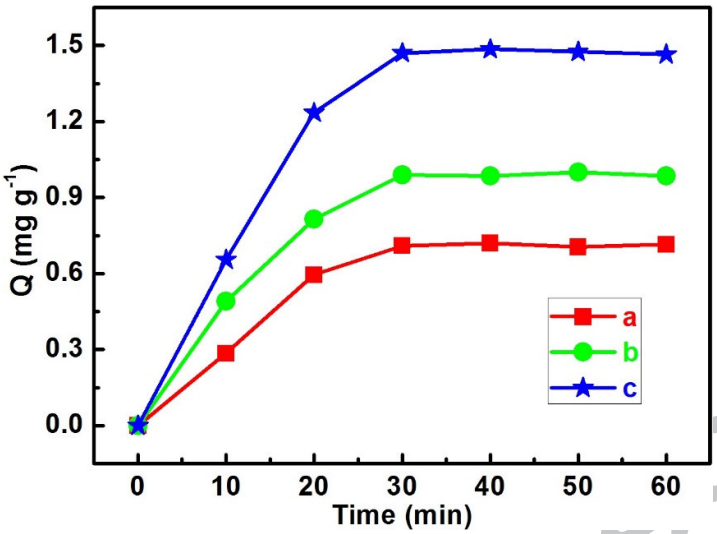

Fig. 8 Adsorption of $ZnFe_2O_4$ (a), Ag/PEDOT (b) and Z-scheme imprinted $ZnFe_2O_4$/Ag/PEDOT (c) (conditions: sample dose: 0.002 g L^{-1}, TC concentration: 20 mg L^{-1}, pH: 5.93)

3.3 Influence of different adding doses of Ag/PEDOT and different microwave polymerization times on photocatalytic activity

The influence of different adding doses of Ag/PEDOT (0.001 g, 0.005 g, 0.01 g, 0.05 g and 0.1 g) and different microwave polymerization times (0.1 h, 0.5 h, 1 h, 1.5 h and 2 h) on the photocatalytic activity of the Z-scheme imprinted $ZnFe_2O_4$/Ag/PEDOT were also investigated to achieve a better photocatalytic activity. As shown in Fig. 9A, 0.01 g was the optimal adding doses of Ag/PEDOT, and the photodegradation rate of Z-scheme imprinted $ZnFe_2O_4$/Ag/PEDOT reached 71.77 %. When the adding dose of Ag/PEDOT was less than 0.01 g, it can be clearly seen that the higher the content of Ag/PEDOT, the better the photocatalytic activity of Z-scheme imprinted $ZnFe_2O_4$/Ag/PEDOT. While when the adding dose of Ag/PEDOT was more than 0.01 g, due to the excessive Ag/PEDOT, the surface imprinted layer would become thicker, which would make the transmission of the electrons and holes became slow, and this further resulted in the lower photocatalytic activity. In addition, it can be easily found that in Fig. 9B that 1 h was the optimal microwave polymerization time to synthesize the Z-scheme imprinted $ZnFe_2O_4$/Ag/PEDOT. If the microwave polymerization time was less than 1 h, the polymerization would not complete and the imprinted layer would not fully form, which would lead to the decrease of the photocatalytic activity. While if the microwave polymerization time was more than 1 h, the polymerization degree would increase, which would lead to: (i) the thicker surface

imprinted layer, and the less distribution of the imprinted cavities on the surface, (ii) the more stable bonding degree which was detrimental to the removal and re-binding of TC, both of the two reasons would lead to a decrease in the photocatalytic activity. Therefore, in the following experiments, 0.01 g was chosen as the adding dose of Ag/PEDOT, and 1 h was chosen as the microwave polymerization time. What's more, the corresponding plots of $\ln(C_o/C)$ versus hν time was displayed in Fig. S1, and the corresponding apparent rate constants (Table S1 and Table S2) were calculated according to the equation (8) [66, 67]. It can be easily found that all the data in Table S1 and Table S2 were in accordance with the above results.

$$\ln (C_o/C) = kt \quad (8)$$

Where C_o is the initial concentration of TC after adsorbing, C is the concentration of TC after irradiating, k is the apparent rate constant and t is the irradiation time.

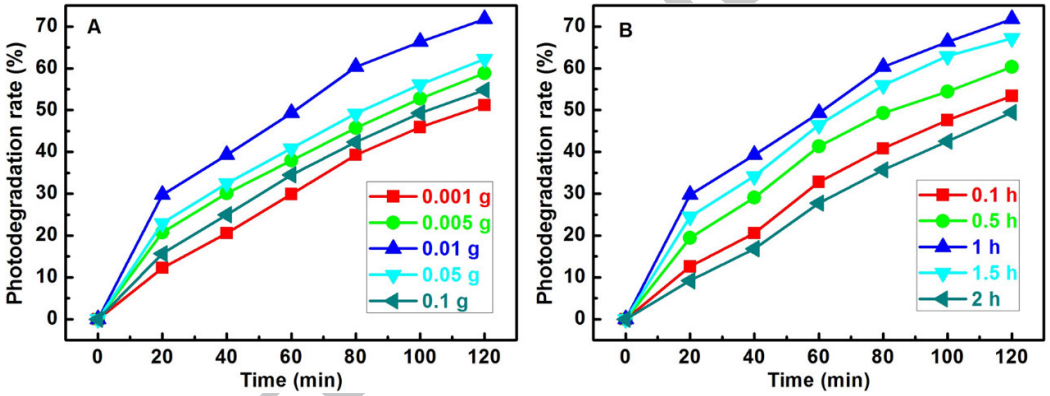

Fig. 9 Influence of different adding doses of Ag/PEDOT (A) and different microwave polymerization times (B) for synthesizing the Z-scheme imprinted $ZnFe_2O_4$/Ag/PEDOT on the photocatalytic activity (conditions: sample dose: 0.002 g L^{-1}, TC concentration: 20 mg L^{-1}, pH: 5.93)

3.4 Selectivity

The photocatalytic activity of photodegradation of the single antibiotic solution was compared to investigate the selectivity of different samples, which was shown in Fig. 10. It can be easily found that $ZnFe_2O_4$ possessed very poor photocatalytic activity, after the simulated sunlight irradiation for 120 min, the photodegradation rate was only 15.14 % for TC and 19.91 % for EH. While Ag/PEDOT had a relatively good photocatalytic activity, which may rely on the photo-generated electrons transfer effect of Ag. Compared with Ag/PEDOT, the photocatalytic activity of photodegradation of TC and EH with non-imprinted $ZnFe_2O_4$/Ag/PEDOT was better,

which fully proved that the Z-scheme structure indeed enhanced the photocatalytic activity. What's more, because that Z-scheme imprinted $ZnFe_2O_4$/Ag/PEDOT had a lot of imprinted cavities in the surface imprinted layer, and these imprinted cavities possessed strong affinity to TC, accordingly, for photodegradation of TC, Z-scheme imprinted $ZnFe_2O_4$/Ag/PEDOT possessed the highest photodegradation rate (71.77 %) under the simulated sunlight irradiation of 120 min, which was approximately 4.74 times to that of $ZnFe_2O_4$, 1.42 times to that of Ag/PEDOT and 1.31 times to that of non-imprinted $ZnFe_2O_4$/Ag/PEDOT, respectively, besides, due to the relatively large structural difference between TC and EH, the imprinted cavities can not efficient specific recognition of EH, consequently, for photodegradation of EH, Z-scheme imprinted $ZnFe_2O_4$/Ag/PEDOT possessed the relatively poor photodegradation rate.

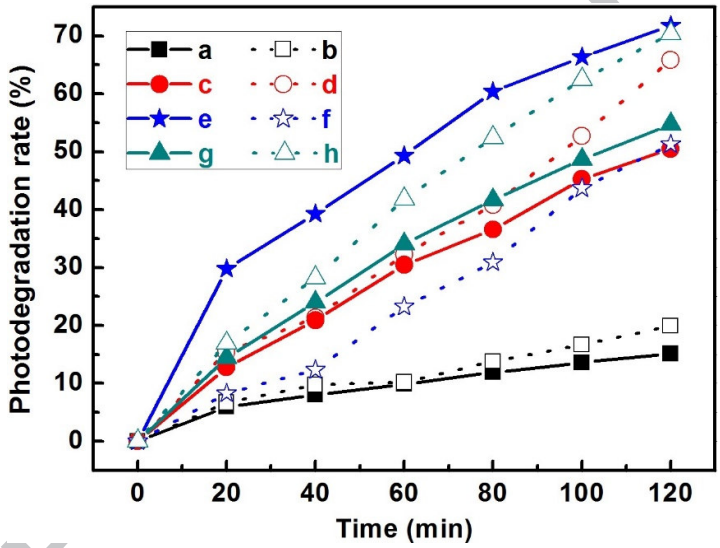

Fig. 10 Selectivity for photodegradation of the single antibiotic solution with different samples under the simulated sunlight irradiation of 120 min (a and b: $ZnFe_2O_4$; c and d: Ag/PEDOT; e and f: Z-scheme imprinted $ZnFe_2O_4$/Ag/PEDOT; g and h: non-imprinted $ZnFe_2O_4$/Ag/PEDOT) (a, c, e and g: degradation of TC; b, d, f and h: degradation of EH) (conditions: sample dose: 0.002 g L^{-1}, TC concentration: 20 mg L^{-1}, EH concentration: 20 mg L^{-1}, pH of TC solution: 5.93, pH of EH solution: 5.49)

The detailed photodegradation rates and coefficients of selectivity of different samples for photodegradation of the single antibiotic solution were presented in Table 1. It can be clearly seen that coefficient of selectivity ($k_{selectivity}$) of Z-scheme imprinted $ZnFe_2O_4$/Ag/PEDOT relative to $ZnFe_2O_4$, Ag/PEDOT and non-imprinted $ZnFe_2O_4$/Ag/PEDOT was 1.84, 1.82 and 1.79,

respectively, which demonstrated that $k_{selectivity}$ mainly depended on the structure of TC, and Z-scheme imprinted $ZnFe_2O_4$/Ag/PEDOT possessed the imprinted cavities which can effective selective photodegradation of TC in the presence of EH.

Table 1 Photodegradation rates and coefficients of selectivity for degradation of the single antibiotic solution with different samples under the simulated sunlight irradiation of 120 min (conditions: sample dose: 0.002 g L^{-1}, TC concentration: 20 mg L^{-1}, EH concentration: 20 mg L^{-1}, pH of TC solution: 5.93, pH of EH solution: 5.49)

Sample	Antibiotic solution	Photodegradation rate (%)	$k_{imprinted}$	k_{others}	$k_{selectivity}$
$ZnFe_2O_4$	TC	15.14	—	0.76	1.84
	EH	19.91			
Ag/PEDOT	TC	50.51	—	0.77	1.82
	EH	65.86			
Z-scheme imprinted $ZnFe_2O_4$/Ag/PEDOT	TC	71.77	1.4	—	—
	EH	51.26			
Non-imprinted $ZnFe_2O_4$/Ag/PEDOT	TC	54.76	—	0.78	1.79
	EH	70.36			

The selective experiment in binary antibiotic solution containing TC and EH was carried out to further investigate the selectivity of different samples. As displayed in Fig. 11 and Table 2, the degradation trend of different samples in binary antibiotic solution was almost consistent with that in the single antibiotic solution. However, the photodegradation rate of the same sample for degradation of the binary antibiotic solution was much lower than that of the single antibiotic solution, which was because regardless of the binary antibiotic solution and the single antibiotic solution, the sample dose was the same (0.002 g L^{-1}), while the antibiotic concentration was different, the binary antibiotic solution contained two kinds of antibiotics, accordingly, the photodegradation rate of the same sample for degradation of the binary antibiotic solution was much lower than that of the single antibiotic solution. On the other hand, it can be clearly seen that, for degradation of the binary antibiotic solution, the coefficient of selectivity ($k_{selectivity}$) of

Z-scheme imprinted $ZnFe_2O_4$/Ag/PEDOT relative to $ZnFe_2O_4$, Ag/PEDOT and non-imprinted $ZnFe_2O_4$/Ag/PEDOT was 1.78, 1.75 and 1.67, respectively. All above results further proved that the Z-scheme imprinted $ZnFe_2O_4$/Ag/PEDOT not only possessed high photocatalytic efficiency, but also had the specific recognition ability for selective photodegradation of TC both in the single antibiotic solution and the binary antibiotic solution.

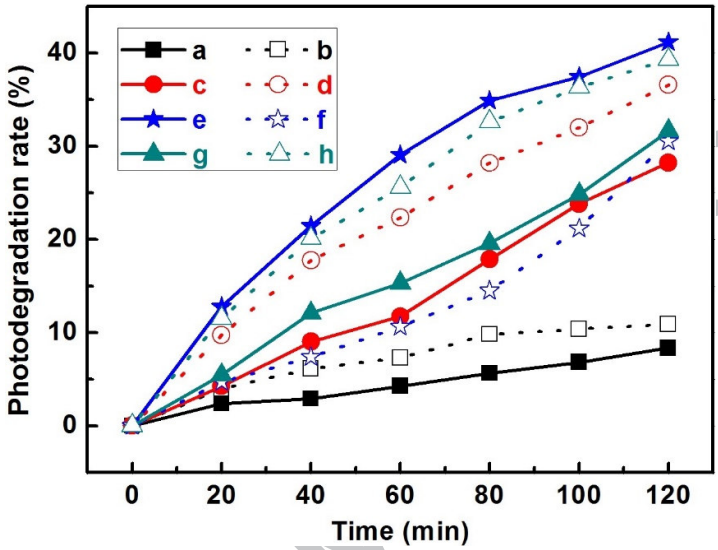

Fig. 11 Selectivity for photodegradation of the binary antibiotic solution containing TC (a, c, e and g) and EH (b, d, f and h) with different samples under the simulated sunlight irradiation of 120 min (a and b: $ZnFe_2O_4$, c and d: Ag/PEDOT, e and f: Z-scheme imprinted $ZnFe_2O_4$/Ag/PEDOT, g and h: non-imprinted $ZnFe_2O_4$/Ag/PEDOT) (conditions: sample dose: 0.002 g L^{-1}, TC concentration in the binary antibiotic solution: 20 mg L^{-1}, EH concentration in the binary antibiotic solution: 20 mg L^{-1}, pH: 5.66)

Table 2 Photodegradation rates and coefficients of selectivity for degradation of the binary antibiotic solution containing TC and EH with different samples under the simulated sunlight irradiation of 120 min (conditions: sample dose: 0.002 g L^{-1}, TC concentration in the binary antibiotic solution: 20 mg L^{-1}, EH concentration in the binary antibiotic solution: 20 mg L^{-1}, pH: 5.66)

Sample	Antibiotic solution	Photodegradation rate (%)	$k_{imprinted}$	k_{others}	$k_{selectivity}$
$ZnFe_2O_4$	TC	8.23	—	0.76	1.78
	EH	10.90			

Ag/PEDOT	TC	28.23	—	0.77	1.75
	EH	36.58			
Z-scheme imprinted $ZnFe_2O_4$/Ag/PEDOT	TC	41.16	1.35	—	—
	EH	30.54			
Non-imprinted $ZnFe_2O_4$/Ag/PEDOT	TC	31.63	—	0.81	1.67
	EH	39.28			

3.5 Reproducibility

Fig. 12 displayed the reproducibility of the Z-scheme imprinted $ZnFe_2O_4$/Ag/PEDOT by 5 cycles. It can be easily found in Fig. 12A that Z-scheme imprinted $ZnFe_2O_4$/Ag/PEDOT could be used at least 5 cycles with a little loss of photocatalytic activity, demonstrating that the Z-scheme imprinted $ZnFe_2O_4$/Ag/PEDOT had good photocatalytic stability and reproducibility. Besides, as displayed in Fig. 12B, the XRD pattern of the sample after 5 cycles was nearly the same with that of the initial sample, demonstrating that the crystalline structure of the Z-scheme imprinted $ZnFe_2O_4$/Ag/PEDOT was not changed during the photocatalytic reaction.

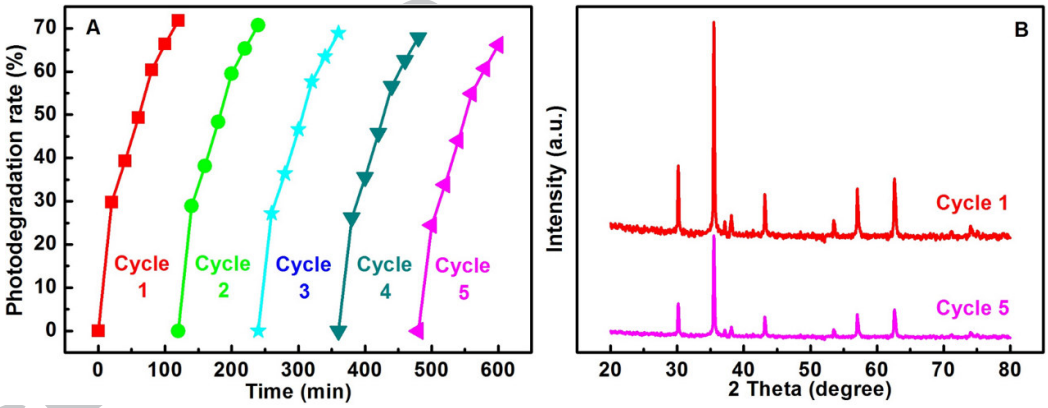

Fig. 12 Photodegradation rates (A) and XRD patterns (B) of the Z-scheme imprinted $ZnFe_2O_4$/Ag/PEDOT with different cycles (photocatalytic experimental conditions: sample dose: 0.002 g L^{-1}, TC concentration: 20 mg L^{-1}, pH: 5.93)

3.6 Mechanism

As everyone knows, the photocatalytic active species (such as h^+, $\cdot OH$, and $\cdot O_2^-$) played a very important role in the photocatalytic reaction [64, 68, 69]. Therefore, the corresponding experiment of the Z-scheme imprinted $ZnFe_2O_4$/Ag/PEDOT was carried out in accordance with

part 2.7, and the results were shown in Fig. 13. During the photocatalytic process, TEOA, t-BuOH and BQ were used as the quenchers for h^+, ·OH and $\cdot O_2^-$, respectively. It can be clearly seen that the photocatalytic activity was seriously affected by adding TEOA and the photodegradation rate was only 20.75 %, indicating that h^+ played a key role on the photocatalytic activity of Z-scheme imprinted $ZnFe_2O_4$/Ag/PEDOT. In contrast, compared with that without quencher (71.77 %), the photodegradation rate reduced to 59.86 % and 50.85 % by adding t-BuOH and BQ, respectively, which demonstrated that ·OH and $\cdot O_2^-$ played a small role on the photocatalytic activity of Z-scheme imprinted $ZnFe_2O_4$/Ag/PEDOT.

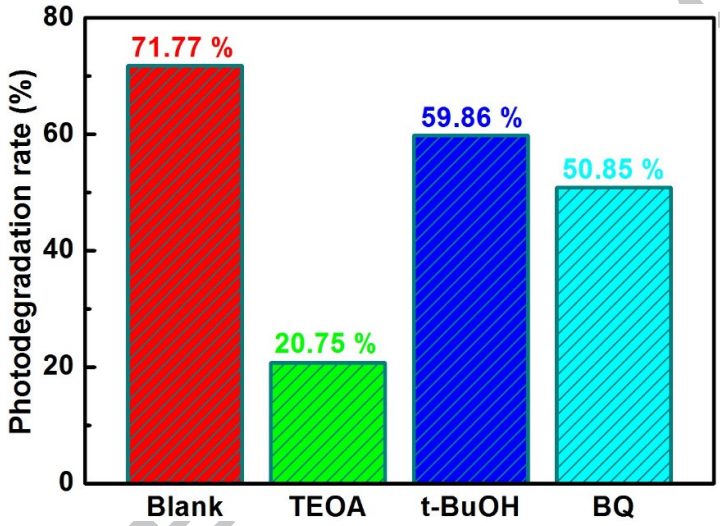

Fig. 13 Photodegradation rates for degradation of TC with the Z-scheme imprinted $ZnFe_2O_4$/Ag/PEDOT in the presence of different quenchers under the simulated sunlight irradiation of 120 min (conditions: sample dose: 0.002 g L^{-1}, TC concentration: 20 mg L^{-1}, pH: 5.93)

Interestingly, based on above data, we found that the role of ·OH was smaller than that of $\cdot O_2^-$, which implied that h^+ may not react with H_2O/OH^- to form ·OH, and the ·OH may be only generated form $\cdot O_2^-$. In order to further confirm above conjecture, Mott–Schottky experiment was conducted to evaluate the band positions of $ZnFe_2O_4$ and PEDOT (Fig. 14). It can be easily found that, both the slope of linear C^{-2} potential curve was positive in Fig. 14A and Fig. 14B, indicating that $ZnFe_2O_4$ and PEDOT were all belong to n-type material. Moreover, the flat band potential of $ZnFe_2O_4$ and PEDOT was -0.98 V vs. Ag/AgCl and -0.67 V vs. Ag/AgCl, respectively. According to the Nernst equation (Equation 9) [70], the flat band potential of $ZnFe_2O_4$ and PEDOT can be

calculated to -0.06 V vs. NHE and -0.37 V vs. NHE.

$$E_{NHE}=E_{Ag/AgCl}+0.059\times pH+E^{\theta}_{Ag/AgCl} \quad (9)$$

Where E_{NHE}, $E_{Ag/AgCl}$ and $E^{\theta}_{Ag/AgCl}$ were the converted applied potential (vs. NHE), the applied potential (vs. Ag/AgCl) and the standard Ag/AgCl electrode potential at 25 ^{o}C (0.197 V), respectively. The pH for the electrolyte was 7.02.

It is known that the conduction bands of n-type semiconductors are 0 eV - 0.1 eV higher than the flat potentials [71]. Here, the voltage difference between the conduction band (CB) and the flat potential was set to be 0.05 eV [71], therefore, the estimated positions of conduction band (CB) of $ZnFe_2O_4$ and LUMO energy level of PEDOT were -0.42 eV vs. NHE and -0.11 eV vs. NHE, respectively. According to the results of Fig. 6, the band gap (E_g) of $ZnFe_2O_4$ and PEDOT was 2.03 eV, and 2.21 eV, respectively. Therefore, the conduction band (CB) and valence band (VB) of $ZnFe_2O_4$ were -0.42 eV and 1.61 eV, respectively, and the LUMO energy level and HOMO energy level of PEDOT were -0.11 eV and 2.1 eV, respectively. Consequently, based on the VB position of $ZnFe_2O_4$ and the HOMO energy level position of PEDOT, above conjecture that ·OH was only generated form $\cdot O_2^-$ had been confirmed.

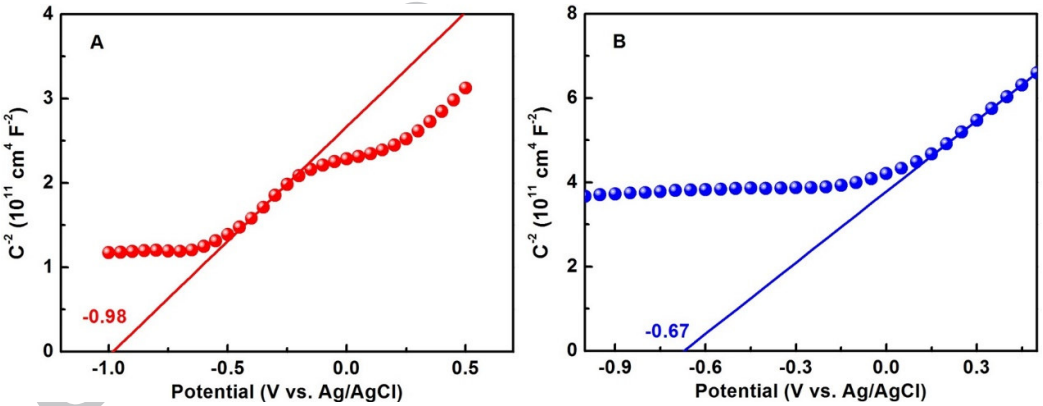

Fig. 14 Mott-Schottky plots for $ZnFe_2O_4$ electrode (A) and PEDOT electrode (B) in 0.5 M Na_2SO_4 aqueous solution (pH = 7.02)

More importantly, due to the existence of Ag between $ZnFe_2O_4$ and PEDOT and the energy level positions of $ZnFe_2O_4$ and PEDOT, the Z-scheme structure may be formed in this photocatalytic system. In order to prove the Z-scheme structure, the production of $\cdot O_2^-$ and ·OH was further detected by the ESR technique. As shown in Fig. 15, no signal was found in the spectrum of PEDOT, indicating that PEDOT can not generate $\cdot O_2^-$. Moreover, the signal intensity

of Z-scheme imprinted $ZnFe_2O_4$/Ag/PEDOT were stronger than that of $ZnFe_2O_4$, this result indicated that $ZnFe_2O_4$ and Z-scheme imprinted $ZnFe_2O_4$/Ag/PEDOT can not only generate $\cdot O_2^-$, but also the amounts of $\cdot O_2^-$ generated from Z-scheme imprinted $ZnFe_2O_4$/Ag/PEDOT were larger than that from $ZnFe_2O_4$ [72]. The cause of the above results must be that the electrons (e^-) generated from the LUMO energy level of PEDOT was transferred to Ag and further combined with the hole (h^+) transferred from the VB energy level of $ZnFe_2O_4$ to Ag. Because if the e^- generated from the CB energy level of $ZnFe_2O_4$ transferred to Ag and further to PEDOT or the e^- generated from the CB energy level of $ZnFe_2O_4$ transferred to PEDOT and further to Ag, due to the fact that the reaction could not occur to generate $\cdot O_2^-$ on the LUMO energy level of PEDOT, the characteristic peaks with relative intensity corresponding to DMPO–$\cdot O_2^-$ of Z-scheme imprinted $ZnFe_2O_4$/Ag/PEDOT would not be higher than that of $ZnFe_2O_4$, hence the conclusion of this hypothesis was inconsistent with the results in Fig. 15. Similarly, due to the fact that $\cdot$OH was only generated form $\cdot O_2^-$, the ESR spectra of DMPO–$\cdot$OH had the same trend with the ESR spectra of DMPO–$\cdot O_2^-$, the results were showed in Fig. S2. In addition, due to the positions of valence band (VB) of $ZnFe_2O_4$ (1.61 eV) and HUMO energy level of PEDOT (2.1 eV), the hole (h^+) generated from the VB energy level of $ZnFe_2O_4$ can not transfer to the HUMO energy level of PEDOT, and the h^+ can not react with H_2O/OH^- to form $\cdot$OH both in the valence band (VB) of $ZnFe_2O_4$ and HUMO energy level of PEDOT. Therefore, in this work, the electrons (e^-) generated from the LUMO energy level of PEDOT was transferred to Ag and further combined with the hole (h^+) transferred from the VB energy level of $ZnFe_2O_4$ to Ag. Obviously, the Z-scheme structure had been formed.

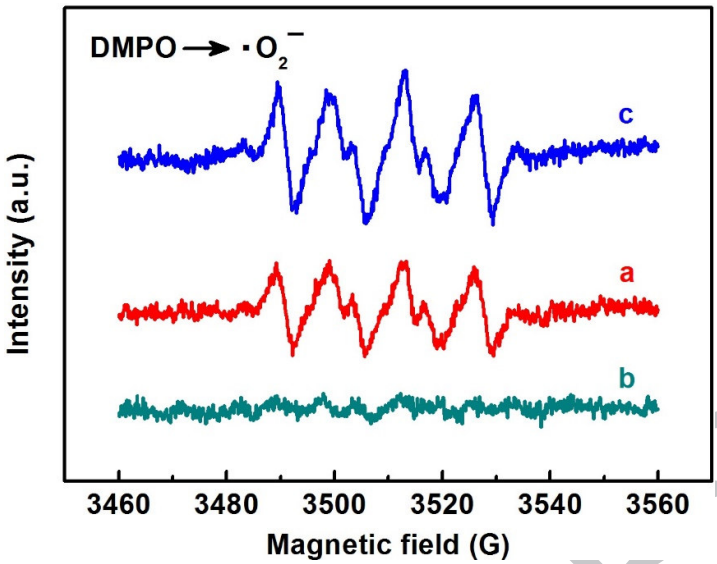

Fig. 15 ESR signals DMPO−·O_2^- with visible light irradiation of $ZnFe_2O_4$ (a), PEDOT (b) and Z-scheme imprinted $ZnFe_2O_4$/Ag/PEDOT (c).

Combined with all the above results, the photocatalytic and selective mechanism of the Z-scheme imprinted $ZnFe_2O_4$/Ag/PEDOT was proposed and presented in Fig. 16. Briefly, due to the existence of imprinted cavity in the surface layer, TC can be specifically recognized and further selectively photodegraded, similarly, owing to the relatively large structural difference between TC and EH, the imprinted cavities can not efficient specific recognition of EH. Therefore, the specific recognition and selective photodegradation was realized through the imprinted cavity. And when the Z-scheme imprinted $ZnFe_2O_4$/Ag/PEDOT was exposed to simulated sunlight, the electrons (e^-) and holes (h^+) were generated respectively in the corresponding energy level of $ZnFe_2O_4$ and PEDOT. Subsequently, due to the existence of Ag between $ZnFe_2O_4$ and PEDOT, the e^- generated from the LUMO energy level of PEDOT and the h^+ generated from the VB energy level of $ZnFe_2O_4$ both transferred to Ag, consequently, the e^- in the CB energy level of $ZnFe_2O_4$ were captured by dissolved O_2 to generate $\cdot O_2^-$, and further generated ·OH, meanwhile, the h^+ generated from the HOMO energy level of PEDOT directly oxidized TC to generate CO_2, H_2O and other molecules.

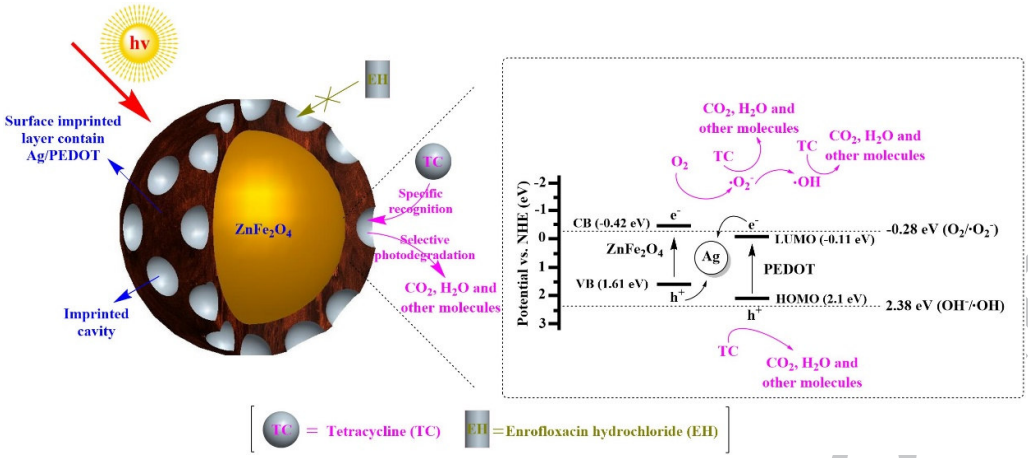

Fig. 16 Proposed photocatalytic and selective mechanism of the Z-scheme imprinted $ZnFe_2O_4$/Ag/PEDOT

3.7 Photodegradation intermediates analysis

The mineralization degree of photodegradation of TC with the Z-scheme imprinted $ZnFe_2O_4$/Ag/PEDOT was investigated in accordance with part 2.9. As shown in Fig. S3, the mineralization rate was only 44.56 %, which was much lower than its photodegradation rate (71.77 %), above result indicated that a lot of photodegradation intermediates were generated during the photocatalytic reaction. In order to further investigate the photodegradation process in depth, MS was employed to identify the photodegradation intermediates, which was displayed in Fig. S4. Through an in-depth analysis and comparison of Fig.S4A, Fig. S4B and Fig. S4C, the possible photodegradation intermediates were inferred. As displayed in Fig. 17, TC may first occur the addition reaction and further lose the group of $–CONH_2$ to form A (m/z = 455) and D (m/z = 412), or first lose the group of $–CONH_2$ and further occur the addition reaction to form B (m/z = 402) and D (m/z = 412). Afterwards, B (m/z = 402) may lose the group of $–N(CH_3)_2$ to form C (m/z = 359), and then occur the addition reaction to form E (m/z = 369). Meanwhile, D (m/z = 412) may also lose the group of $–N(CH_3)_2$ to form E (m/z = 369). Subsequently, E (m/z = 369) may be fragmented into F (m/z = 343) by leaving the group of –C=O, and F (m/z = 343) may be further fragmented into G (m/z = 285) by leaving the group of $–CH_2CH(OH)CH_3$. Nevertheless, because the reaction time was short, TC was not completely degraded, while if the reaction time was extended, all the photodegradation intermediates would be degraded to CO_2, H_2O and other molecules.

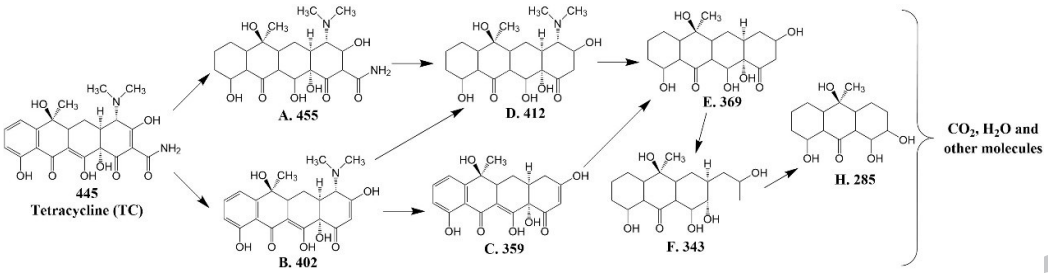

Fig.17 Possible intermediates analysis of photodegradation of TC with the Z-scheme imprinted $ZnFe_2O_4$/Ag/PEDOT

4. Conclusions

In brief, the Z-scheme imprinted $ZnFe_2O_4$/Ag/PEDOT was synthesized based on $ZnFe_2O_4$ as the carrier and Ag/PEDOT as the functional monomer by the microwave polymerization method and surface imprinting technique, the optimal adding doses of Ag/PEDOT was 0.01 g and the optimal microwave polymerization time was 1 h. The experimental results demonstrated that the as-prepared Z-scheme imprinted $ZnFe_2O_4$/Ag/PEDOT possessed good partial hollow spherical structure, good light response ability, good magnetic separation performance, good photocatalytic stability and reproducibility. Moreover, based on the electrochemical analysis with the Mott–Schottky experiments and UV-vis DRS spectra with the corresponding Kubelca-Munk equation, and also combined with the results of photocatalytic experiments by adding different quenchers, the photocatalytic mechanism was confirmed that due to the introduction of Ag/PEDOT into the surface imprinted layer, Ag acted as the mediator, Z-scheme structure was formed to enhance the photocatalytic activity. Accordingly, the photodegradation rate of Z-scheme imprinted $ZnFe_2O_4$/Ag/PEDOT for degradation of TC under the simulated sunlight irradiation of 120 min was 71.77 %, which was approximately 4.74 times to that of $ZnFe_2O_4$, 1.42 times to that of Ag/PEDOT and 1.31 times to that of non-imprinted $ZnFe_2O_4$/Ag/PEDOT, respectively. Meanwhile, owing to the existence of the imprinted cavity in the surface imprinted layer, the selectivity had been significantly improved. The coefficient of selectivity of Z-scheme imprinted $ZnFe_2O_4$/Ag/PEDOT relative to $ZnFe_2O_4$, Ag/PEDOT, non-imprinted $ZnFe_2O_4$/Ag/PEDOT was 1.84, 1.82, 1.79 in the single antibiotic solution and 1.78, 1.75, 1.67 in the binary antibiotic solution, respectively. In a word, the as-prepared Z-scheme imprinted $ZnFe_2O_4$/Ag/PEDOT not only possessed good photocatalytic activity, but also exhibited the superior specific recognition

ability for selective photodegradation of TC. This work provided a new synthesis strategy for the imprinted photocatalysts and also provided a new idea for the treatment of specific pollutants in the water environment.

Acknowledgements

This work was financially supported by the National Natural Science Foundation of China (No. 21607062), the Natural Science Foundation of Jiangsu Province (Nos. BK20160494, BK20140532 and BK20150536), the China Postdoctoral Science Foundation (Nos. 2016M600378 and 2017T100333), the Social Development Project of Key Research Program of Zhenjiang (No. SH2016018), the Youth Talent Development Program of Jiangsu University and the Jiangsu Collaborative Innovation Center of Technology and Material of Water Treatment.

References

[1] G.G. Liu, K. Han, H.Q. Ye, C.Y. Zhu, Y.P. Gao, Y. Liu, Y.H. Zhou, Graphene oxide/triethanolamine modified titanate nanowires as photocatalytic membrane for water treatment, Chem. Eng. J. 320 (2017) 74–80.

[2] C. Santhosh, V. Velmurugan, G. Jacob, S.K. Jeong, A.N. Grace, A. Bhatnagar, Role of nanomaterials in water treatment applications: A review, Chem. Eng. J. 306 (2016) 1116–1137.

[3] Z.Y. Lu, P.W. Huo, Y.Y. Luo, X.L. Liu, D. Wu, X. Gao, C.X. Li, Y.S. Yan, Performance of molecularly imprinted photocatalysts based on fly-ash cenospheres for selective photodegradation of single andternary antibiotics solution, J. Mol. Catal. A–Chem. 378 (2013) 91–98.

[4] K.H. Chu, Y.A.J. Al-Hamadani, C.M. Park, G. Lee, M. Jang, A. Jang, N. Her, A. Son, Y. Yoon, Ultrasonic treatment of endocrine disrupting compounds, pharmaceuticals, and personal care products in water: A review, Chem. Eng. J. 327 (2017) 629–647.

[5] Z. Zhu, X. Tang, S. Kang, P.W. Huo, M.S. Song, W.D. Shi, Z.Y. Lu, Y.S. Yan, Constructing of the Magnetic Photocatalytic Nanoreactor MS@FCN for Cascade Catalytic Degrading of Tetracycline, J. Phys. Chem. C 120 (2016) 27250–27258.

[6] F. Guo, W.L. Shi, H.B. Wang, M.M. Han, H. Li, H. Huang, Y. Liu, Z.H. Kang, Facile fabrication of a CoO/g-C_3N_4 p–n heterojunction with enhanced photocatalytic activity and stability for tetracycline degradation under visible light, Catal. Sci. Technol. 7 (2017) 3325–3331.

[7] J.Q. Lou, X. Xu, Y.F. Gao, D.Z. Zheng, J.Y. Wang, Z.G. Li, Preparation of magnetic activated carbon from waste rice husk for the determination of tetracycline antibiotics in water samples, RSC Adv. 6 (2016) 112166–112174.

[8] S. Azimi, A. Nezamzadeh-Ejhieh, Enhanced activity of clinoptilolite-supported hybridized PbS–CdS semiconductors for the photocatalytic degradation of a mixture of tetracycline and cephalexin aqueous solution, J. Mol. Catal. A–Chem. 408 (2015) 152–160.

[9] A. Nezamzadeh-Ejhieh, A. Shirzadi, Enhancement of the photocatalytic activity of Ferrous Oxide by doping onto the nano-clinoptilolite particles towards photodegradation of tetracycline, Chemosphere 107 (2014) 136–144.

[10] X.N. Wang, J.P. Jia, Y.L. Wang, Combination of photocatalysis with hydrodynamic cavitation for degradation of tetracycline, Chem. Eng. J. 315 (2017) 274–282.

[11] Z.Y. Lu, Z. Zhu, D.D. Wang, Z.F. Ma, W.D. Shi, Y.S. Yan, X.X. Zhao, H.J. Dong, L. Yang, Z.F. Hua, Specific oriented recognition of a new stable ICTX@Mfa with retrievability for selectively photocatalytic degrading ciprofloxacin, Catal. Sci. Technol. 6 (2016) 1367–1377.

[12] J.J. Wang, L. Tang, G.M. Zeng, Y.N. Liu, Y.Y. Zhou, Y.C. Deng, J.J. Wang, B. Peng, Plasmonic Bi Metal Deposition and g□C_3N_4 Coating on Bi_2WO_6 Microspheres for Efficient Visible-Light Photocatalysis, ACS Sustain. Chem. Eng. 5 (2017) 1062−1072.

[13] G.Z. Yuan, C.F. Hsia, Z.W. Lin, C. Chiang, Y.W. Chiang, M.H. Huang, Highly Facet-Dependent Photocatalytic Properties of Cu_2O Crystals Established through the Formation of Au-Decorated Cu_2O Heterostructures, Chem. Eur. J. 22 (2016) 12548–12556.

[14] Z.Y. Lu, X.X. Zhao, Z. Zhu, Y.S. Yan, W.D. Shi, H.J. Dong, Z.F. Ma, N.L. Gao, Y.S. Wang, H. Huang, Enhanced recyclability, stability and selectivity of CdS/C@Fe_3O_4 nanoreactor for orientation photodegradation of ciprofloxacin, Chem. Eur. J. 21 (2015) 18528–18533.

[15] P.F. Feng, J.P. Zhao, J.C. Zhang, Y.D. Wei, Y.N. Wang, H.H. Li, Y.H. Wang, Long persistent photocatalysis of magnesium gallate nanorodes, J. Alloy. Compd. 695 (2017) 1884–1890.

[16] S.N. Liu, M. Zheng, R. Chen, Z.S. Wang, One-pot synthesis of an AgBr/ZnO hierarchical structure with enhanced photocatalytic capacity, RSC Adv. 7 (2017) 31230–31238.

[17] Z.Y. Lu, W.C. Zhou, P.W. Huo, Y.Y. Luo, M. He, J.M. Pan, C.X. Li, Y.S. Yan, Performance of a novel TiO_2 photocatalyst based on the magnetic floating fly-ash cenospheres for the purpose of treating waste by waste, Chem. Eng. J. 225 (2013) 34–42.

[18] M. Pelaez, P. Falaras, V. Likodimos, K. O'Shea, A.A. de la Cruz, P.S.M. Dunlop, J.A. Byrne, D.D. Dionysiou, Use of selected scavengers for the determination of NF-TiO_2 reactive oxygen species during the degradation of microcystin-LR under visible light irradiation, J. Mol. Catal. A–Chem. 425 (2016) 183–189.

[19] H.W. Bai, Z.Y. Liu, L. Liu, D.D. Sun, Large-Scale Production of Hierarchical TiO_2 Nanorod Spheres for Photocatalytic Elimination of Contaminants and Killing Bacteria, Chem. Eur. J. 19 (2013) 3061–3070.

[20] S.S. Fang, M.Y. Sun, Y.W. Zhou, Q. Liang, Z.Y. Li, S. Xu, Solvothermal synthesis of CdS QDs/MWCNTs nanocomposites with high efficient photocatalytic activity under visible light irradiation, J. Alloy. Compd. 656 (2016) 771–776.

[21] X.L. Song, Y.Y. Li, Z.D. Wei, S.Y. Ye, D.D. Dionysiou, Synthesis of $BiVO_4$/P25 composites for the photocatalytic degradation of ethylene under visible light, Chem. Eng. J. 314 (2017) 443–452.

[22] M. Pelaez, N.T. Nolan, S.C. Pillai, M.K. Seery, P. Falaras, A.G. Kontos, P.S.M. Dunlop, J.W.J. Hamilton, J.A. Byrne, K. O'Shea, M.H. Entezari, D.D. Dionysiou, A review on the visible light active titanium dioxide photocatalysts for environmental applications, Appl. Catal., B 125 (2012) 331–349.

[23] C. Boitard, A.L. Rollet, C. Ménager, N. Griffete, Surface-Initiated Synthesis of Bulk-Imprinted Magnetic Polymer for Protein Recognition, Chem. Commun. 53 (2017) 8846–8849.

[24] R.Z. Wang, D.L. Huang, Y.G. Liu, Z.W. Peng, G.M. Zeng, C. Lai, P. Xu, C. Huang, C. Zhang, X.M. Gong, Selective removal of BPA from aqueous solution using molecularly imprinted polymers based on magnetic graphene oxide, RSC Adv. 6 (2016) 106201–106210.

[25] H. Song, L.P. Zhu, Y.G. Li, Z.R. Lou, M. Xiao, Z.Z. Ye, Preparation of $ZnFe_2O_4$ nanostructures and highly efficient visible-light-driven hydrogen generation with the assistance of nanoheterostructures, J. Mater. Chem. A 3 (2015) 8353–8360.

[26] F. Zhang, X.Y. Li, Q.D. Zhao, D.K. Zhang, Rational Design of $ZnFe_2O_4/In_2O_3$ Nanoheterostructures: Efficient Photocatalyst for Gaseous 1,2-Dichlorobenzene Degradation and Mechanistic Insight, ACS Sustain. Chem. Eng. 4 (2016) 4554–4562.

[27] S.Q. Liu, X.L. Zhu, Y. Zhou, Z.D. Meng, Z.G. Chen, C.B. Liu, F. Chen, Z.Y. Wu, J.C. Qian,

Smart photocatalytic removal of ammonia through molecular recognition of zinc ferrite/reduced graphene oxide hybrid catalyst under visible-light irradiation, Catal. Sci. Technol. 7 (2017) 3210–3219.

[28] Y.S. Guo, N.S. Zhang, X. Wang, Q.F. Qian, S.Y. Zhang, Z.S. Li, Z.G. Zou, A facile spray pyrolysis method to prepare Ti-doped $ZnFe_2O_4$ for boosting photoelectrochemical water splitting, J. Mater. Chem. A 5 (2017) 7571–7577.

[29] H.B. Chen, W.X. Liu, Z.Z. Qin, $ZnO/ZnFe_2O_4$ nanocomposite as a broad-spectrum photo-Fentonlike photocatalyst with near-infrared activity, Catal. Sci. Technol. 7 (2017) 2236–2244.

[30] C. Lai, M.M. Wang, G.M. Zeng, Y.G. Liu, D.L. Huang, C. Zhang, R.Z. Wang, P. Xu, M. Cheng, C. Huang, H.P. Wu, L. Qin, Synthesis of surface molecular imprinted TiO_2/graphene photocatalyst and its highly efficient photocatalytic degradation of target pollutant under visible light irradiation, Appl. Surf. Sci. 390 (2016) 368–376.

[31] Y.N. Zhang, W.G. Dai, Y.Z. Wen, G.H. Zhao, Efficient enantioselective degradation of the inactive (S)-herbicide dichlorprop on chiral molecular-imprinted TiO_2, Appl. Catal., B 212 (2017) 185–192.

[32] Z.Y. Lu, X.X. Zhao, Z. Zhu, M.S. Song, N.L. Gao, Y.S. Wang, Z.F. Ma, W.D. Shi, Y.S. Yan, H.J. Dong, A novel hollow capsule-like recyclable functional $ZnO/C/Fe_3O_4$ endowed with three-dimensional oriented recognition ability for selectively photodegrading danofloxacin mesylate, Catal. Sci. Technol. 6 (2016) 6513–6524.

[33] Y.Y. Wu, Y.M. Dong, X.F. Xia, X. Liu, H.X. Li, Facile synthesis of N–F codoped and molecularly imprinted TiO_2 for enhancing photocatalytic degradation of target contaminants, Appl. Surf. Sci. 364 (2016) 829–836.

[34] L.X. Chen, X.Y. Wang, W.H. Lu, X.Q. Wu, J.H. Li, Molecular imprinting: perspectives and applications, Chem. Soc. Rev. 45 (2016) 2137–2211.

[35] Y.F. Wang, Y.G. Wang, X.K. Ouyang, L.Y. Yang, Surface-Imprinted Magnetic Carboxylated Cellulose Nanocrystals for the Highly Selective Extraction of Six Fluoroquinolones from Egg Samples, ACS Appl. Mater. Interfaces 9 (2017) 1759–1769.

[36] Z.Y. Lu, M. He, L.L. Yang, Z.F. Ma, L. Yang, D.D. Wang, Y.S. Yan, W.D. Shi, Y. Liu, Z.F. Hua, Selective photodegradation of 2-mercaptobenzothiazole by a novel imprinted

$CoFe_2O_4$/MWCNTs photocatalyst, RSC Adv. 5 (2015) 47820–47829.

[37] R. Yang, Y.X. Liu, X.Y. Yan, S.M. Liu, H.S. Zheng, An Effective Method for the Synthesis of Yolk–Shell Magnetic Mesoporous Carbon–Surface Molecularly Imprinted Microspheres, J. Mater. Chem. A 4 (2016) 9807–9815.

[38] R.M. Liang, J.W. Ding, S.S. Gao, W. Qin, Mussel-Inspired Surface-Imprinted Sensors for Potentiometric Label-Free Detection of Biological Species, Angew. Chem. Int. Ed. 56 (2017) 6833 –6837.

[39] Z.Y. Lu, F. Chen, M. He, M.S. Song, Z.F. Ma, W.D. Shi, Y.S. Yan, J.Z. Lan, F. Li, P. Xiao, Microwave synthesis of a novel magnetic imprinted TiO_2 photocatalyst with excellent transparency for selective photodegradation of enrofloxacin hydrochloride residues solution, Chem. Eng. J. 249 (2014) 15–26.

[40] B.H. Chong, W. Zhu, X.H. Hou, Epitaxial hetero-structure of CdSe/TiO_2 nanotube arrays with PEDOT as a hole transfer layer for photoelectrochemical hydrogen evolution, J. Mater. Chem. A 5 (2017) 6233–6244.

[41] H.Y. Yan, G. Zhang, Y.F. Li, Synthesis and characterization of advanced $Li_3V_2(PO_4)_3$ nanocrystals@conducting polymer PEDOT for high energy lithium-ion batteries, Appl. Surf. Sci. 393 (2017) 30–36.

[42] K. Yuan, L. Chen, Y.W. Chen, In Situ Photocatalytically Heterostructured ZnO-Ag Nanoparticle Composites as Effective Cathode-Modifying Layers for Air-Processed Polymer Solar Cells, Chem. Eur. J. 21 (2015) 11899–11906.

[43] W. Zhang, L. Zhou, H.P. Deng, Ag modified g-C_3N_4 composites with enhanced visible-light photocatalytic activity for diclofenac degradation, J. Mol. Catal. A–Chem. 423 (2016) 270–276.

[44] A.J. Cheah, W.S. Chiu, P.S. Khiew, H. Nakajima, T. Saisopa, P. Songsiriritthigul, S. Radiman, M.A.A. Hamid, Facile synthesis of a Ag/MoS_2 nanocomposite photocatalyst for enhanced visible-light driven hydrogen gas evolution, Catal. Sci. Technol. 5 (2015) 4133–4143.

[45] J. Jiang, H. Li, L.Z. Zhang, New Insight into Daylight Photocatalysis of AgBr@Ag: Synergistic Effectbetween Semiconductor Photoca talysis and Plasmonic Photocatalysis, Chem. Eur. J. 18 (2012) 6360–6369.

[46] A. Meng, J. Xing, Z.J. Li, Q. Wei, Q.D. Li, Ag/AgCl/ZnO nano-networks: Preparation, characterization, mechanism and photocatalytic activity, J. Mol. Catal. A–Chem. 411 (2016)

290–298.

[47] D.Z. Lu, H.M. Wang, X.N. Zhao, K.K. Kondamareddy, J.Q. Ding, C.H. Li, P.F. Fang, Highly Efficient Visible-Light-Induced Photoactivity of Z□Scheme g□C_3N_4/Ag/MoS_2 Ternary Photocatalysts for Organic Pollutant Degradation and Production of Hydrogen, ACS Sustain. Chem. Eng. 5 (2017) 1436−1445.

[48] X.X. Chen, R. Li, X.Y. Pan, X.T. Huang, Z.G. Yi, Fabrication of In_2O_3-Ag-Ag_3PO_4 composites with Z-scheme configuration for photocatalytic ethylene degradation under visible light irradiation, Chem. Eng. J. 320 (2017) 644–652.

[49] H. Derikvandi, A. Nezamzadeh-Ejhieh, Designing of experiments for evaluating the interactions of influencing factors on the photocatalytic activity of NiS and SnS_2: Focus on coupling, supporting and nanoparticles, J. Colloid Interf. Sci. 490 (2017) 628–641.

[50] X.X. Li, T. Wan, J.Y. Qiu, H. Wei, F.H. Qin, Y.H. Wang, Y.J. Liao, Z.Y. Huang, X.C. Tan, In-situ photocalorimetry-fluorescence spectroscopy studies of RhB photocatalysis over Z-scheme g-C_3N_4@Ag@Ag_3PO_4 nanocomposites: A pseudo-zero-order rather than a first-order process, Appl. Catal., B 217 (2017) 591–602.

[51] B.B. Prasad, A. Kumar, R. Singh, Synthesis of novel monomeric graphene quantum dots and corresponding nanocomposite with molecularly imprinted polymer for electrochemical detection of an anticancerous ifosfamide drug, Biosens. Bioelectron. 94 (2017) 1–9.

[52] A.M. Poller, E. Spieker, P.A. Lieberzeit, C. Preininger, Surface Imprints: Advantageous Application of Ready2use Materials for Bacterial Quartz-Crystal Microbalance Sensors, ACS Appl. Mater. Interfaces 9 (2017) 1129−1135.

[53] Z.Y. Lu, Y.Y. Luo, M. He, P.W. Huo, T.T. Chen, W.D. Shi, Y.S. Yan, J.M. Pan, Z.F. Ma, S.Y. Yang, Preparation and performance of a novel magnetic conductive imprinted photocatalyst for selective photodegradation of antibiotic solution, RSC Adv. 3 (2013) 18373–18382.

[54] F. Zhu, L.W. Li, J.D. Xing, Selective adsorption behavior of Cd(II) ion imprinted polymers synthesized by microwave-assisted inverse emulsion polymerization: Adsorption performance and mechanism, J. Hazard. Mater. 321 (2017) 103–110.

[55] H.H. Ji, L. Lyu, L.L. Zhang, X.Q. An, C. Hu, Oxygen vacancy enhanced photostability and activity of plasmon-Ag composites in the visible to near-infrared region for water purification, Appl. Catal., B 199 (2016) 230–240.

[56] Q. Wu, G.E. Chen, W.G. Sun, Z.L. Xu, Y.F. Kong, X.P. Zheng, S.J. Xu, Bio-inspired GO-Ag/PVDF/F127 membrane with improved anti-fouling for natural organic matter (NOM) resistance, Chem. Eng. J. 313 (2017) 450–460.

[57] H.B. Chen, W.X. Liu, Z.Z. Qin, ZnO/$ZnFe_2O_4$ nanocomposite as a broad-spectrum photo-Fenton-like photocatalyst with near-infrared activity, Catal. Sci. Technol. 7 (2017) 2236–2244.

[58] Y. Qu, D. Zhang, X. Wang, H.L. Qiu, T. Zhang, M. Zhang, G. Tian, H.J. Yue, S.H. Feng, G. Chen, Porous $ZnFe_2O_4$ nanospheres as anode materials for Li-ion battery with high performance, J. Alloy. Compd. 721 (2017) 697–704.

[59] T. Yang, H. Wang, X.M. Ou, C.S. Lee, X.H. Zhang, Iodine-Doped-Poly(3,4-Ethylenedioxythiophene)-Modified Si Nanowire 1D Core-Shell Arrays as an Efficient Photocatalyst for Solar Hydrogen Generation, Adv. Mater. 24 (2012) 6199–6203.

[60] N. Srinivasan, Y. Shiga, D. Atarashi, E. Sakai, M. Miyauchi, A PEDOT-coated quantum dot as efficient visible light harvester for photocatalytic hydrogen production, Appl. Catal., B 179 (2015) 113–121.

[61] P.F. Zhang, L. Wang, S.Z. Yang, J.A. Schott, X.F. Liu, S.M. Mahurin, C.L. Huang, Y. Zhang, P.F. Fulvio, M.F. Chisholm, S. Dai, Solid-state synthesis of ordered mesoporous carbon catalysts via a mechanochemical assembly through coordination cross-linking, Nat. Commun. 8 (2017) 15020.

[62] Y.W. Jiang, J.L. Carvalho-de-Souza, R.C.S. Wong, Z.Q. Luo, D. Isheim, X.B. Zuo, A.W. Nicholls, I.W. Jung, J.P. Yue, D.J. Liu, Y.C. Wang, V.D. Andrade, X.H. Xiao, L. Navrazhnykh, D.E. Weiss, X.Y. Wu, D.N. Seidman, F. Bezanilla, B.Z. Tian, Heterogeneous silicon mesostructures for lipid-supported bioelectric interfaces, Nat. Mater. 15 (2016) 1023–1030.

[63] A. Shirzadi, A. Nezamzadeh-Ejhieh, Enhanced photocatalytic activity of supported CuO–ZnO semiconductors towards the photodegradation of mefenamic acidaqueous solution as a semi real sample, J. Mol. Catal. A–Chem. 411 (2016) 222–229.

[64] H. Derikvandi, A. Nezamzadeh-Ejhieh, Synergistic effect of p-n heterojunction, supporting and zeolite nanoparticles in enhanced photocatalytic activity of NiO and SnO_2, J. Colloid Interf. Sci. 490 (2017) 314–327.

[65] Z.G. Yi, J.H. Ye, N. Kikugawa, T. Kako, S.X. Ouyang, H. Stuart-Williams, H. Yang, J.Y.

Cao, W.J. Luo, Z.S. Li, Y. Liu, R.L. Withers, An orthophosphate semiconductor with photooxidation properties under visible-light irradiation, Nat. Mater. 9 (2010) 559–564.

[66] J. Esmaili-Hafshejani, A. Nezamzadeh-Ejhieh, Increased photocatalytic activity of Zn(II)/Cu(II) oxides and sulfides by coupling and supporting them onto clinoptilolite nanoparticles in thedegradation of benzophenone aqueous solution, J. Hazard. Mater. 316 (2016) 194–203.

[67] M.M.J. Sadiq, A.S. Nesaraj, Reflux condensation synthesis and characterization of Co_3O_4 nanoparticles for photocatalytic applications, Iran. J. Catal. 4 (2014) 219–226.

[68] Z.Y. Lu, Z.H. Yu, J.B. Dong, M.S. Song, Y. Liu, X.L. Liu, D. Fan, Z.F. Ma, Y.S. Yan, P.W. Huo, Construction of stable core–shell imprinted Ag-(poly-o-phenylenediamine)/$CoFe_2O_4$ photocatalyst endowed with the specific recognition capability for selective photodegradation of ciprofloxacin, RSC Adv. 7 (2017) 48894–48903.

[69] A. Nezamzadeh-Ejhieh, M. Karimi-Shamsabadi, Decolorization of a binary azo dyes mixture using CuO incorporated nanozeolite-X as a heterogeneous catalyst and solar irradiation, Chem. Eng. J. 228 (2013) 631–641.

[70] P.Y. Kuang, L.Y. Zhang, B. Cheng, J.G. Yu, Enhanced charge transfer kinetics of Fe_2O_3/CdS composite nanorodarrays using cobalt-phosphate as cocatalyst, Appl. Catal., B 218 (2017) 570–580.

[71] G. Yang, D.M. Chen, H. Ding, J.J. Feng, J.Z. Zhang, Y.F. Zhu, S. Hamid, D.W. Bahnemann, Well-designed 3D $ZnIn_2S_4$ nanosheets/TiO_2 nanobelts as direct Z-scheme photocatalysts for CO_2 photoreduction into renewable hydrocarbon fuel with high efficiency, Appl. Catal., B 219 (2017) 611–618.

[72] Z. Zhu, P.W. Huo, Z.Y. Lu, Y.S. Yan, Z. Liu, W.D. Shi, C.X. Li, H.J. Dong, Fabrication of magnetically recoverable photocatalysts using g-C_3N_4 for effective separation of charge carriers through like-Z-scheme mechanism with Fe_3O_4 mediator, Chem. Eng. J. 331 (2018) 615–625.

Highlights

- Z-scheme imprinted $ZnFe_2O_4$/Ag/PEDOT is obtained by microwave and surface imprinting technique.
- The introduction of Ag/PEDOT enhances the photocatalytic activity by forming Z-scheme structure.
- The existence of the imprinted cavity in the surface imprinted layer improves the selectivity.
- The aim for simultaneously improving the photocatalytic activity and selectivity is achieved.

Graphical Abstract

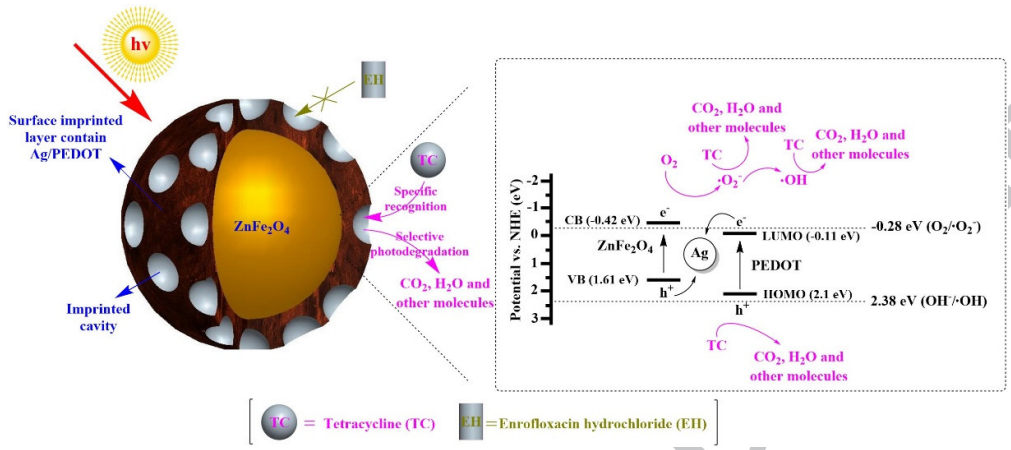

The as-prepared Z-scheme imprinted $ZnFe_2O_4$/Ag/PEDOT achieved the goal for simultaneously improving the photocatalytic activity and selectivity.